DEGREE PROJECT, IN SOLID MECHANICS , SECOND LEVEL
STOCKHOLM, SWEDEN 2015

Stress simulation of the SEAM CubeSat structure during launch

JULIE FAGERUDD

KTH ROYAL INSTITUTE OF TECHNOLOGY

SCHOOL OF ENGINEERING SCIENCES

KTH Engineering Sciences

Stress simulation of the SEAM CubeSat structure during launch

Julie Fagerudd

Degree project in Solid Mechanics
Second level, 30.0 HEC
Stockholm, Sweden 2014

Abstract

A spacecraft is subjected to dynamic and static loads during launch. These loads are deterministic and of random nature and cannot be tested under the real conditions due to cost considerations. The spacecraft must therefore sustain certain mechanical loads without permanent deformation with a certain safety factor due to the uncertainties in the actual loading values during launch. The applicable mechanical test requirements and load combination have been first determined for the structure of interest: the SEAM CubeSat. These requirements are found to be steady-state accelerations, random vibration and shock response spectrum loadings. They have been simulated onto the structure globally and locally in order to extract stress values, amend design features when necessary and determine adequate material properties in order for the final design to fulfill the mechanical requirements during launch.

KTH Teknikvetenskap

Simulering av mekaniska spänningar i nanosatelliten SEAM under uppskjutning

Julie Fagerudd

Examensarbete i Hållfasthetslära
Avancerad nivå, 30 hp
Stockholm, Sverige 2011

Sammanfattning

En satellit utsätts för dynamiska och statiska belastningar under uppskjutningen. Dessa laster är av deterministisk och av slumpmässig natur och kan inte testas under verkliga förhållandena på grund av kostnadsskäl. Satellitens konstruktion måste därför klara at utsättas för utan permanent deformation med en viss säkerhetsfaktor på grund av osäkerheter i de faktiska belastningarna under uppskjutningen. Mekaniska provningskrav och lastkombinationer har bestämts för en utvald struktur: SEAM CubeSat. Dessa krav visar sig vara accelerationer, slumpmässiga vibrationer och stötar. Strukturen har simulerats globalt och lokalt för att få fram de mekaniska belastningarna. Baserat på resultat från simuleringarna har konstruktionen modifierats och lämpliga materialegenskaper har bestämts för att den slutliga konstruktionen ska uppfyllade de mekaniska kraven under uppskjutningen.

Foreword

I would like to thank my supervisor Dr. Gunnar Tibert for his patience, support, for giving me the opportunity to learn more on a fascinating subject and to work on a real engineering project. I would also like to acknowledge Philipp Zimmerhakl for working with me on the CubeSat project. His energy has been a great motivation.

I would like to thank all the department of Solid Mechanics for the help I received and in particular Prashanth Srinivasa for taking the time to enlighten me on random vibrations as well as Dr. Artem Kulachenko whose knowledge in both dynamics and finite elements in general have been a tremendous help.

I would like to thank Dr. Svante Finnveden for his insight on acoustic loading and engineering approach on this problem.

I would like to thank Jonas Nordin from Ansys for his support.

I would finally like to thank Soheil Khoshparvar whose work has been a great source of help.

Finally I would like to thank all my family and particularly my husband and his parents for their support without which my engineering education would not have been possible.

Table of content

1 Introduction

1.1 Spacecraft design requirements

A satellite or spacecraft is exposed to very different loading conditions from its conception on Earth, its launch and finally its release in space. Many different factors such as vibrations, thermal expansion, accelerations can lead to plastic deformations and failure throughout the different stages of a launch. Determination of the appropriate design which could sustain all these loading conditions is crucial for a successful mission.

In order to create a robust spacecraft, the loading conditions need to be identified and quantified in a conservative way. A spacecraft is subjected to static and dynamic loading conditions from lift-off to its release in space. Regarding mechanical loading, the spacecraft needs to sustain loads acting independently or simultaneously:

- Static loading: stresses generating by the assembly of components such as pre-stress in bolts.
- Steady state accelerations: longitudinal and lateral accelerations during lift-off.
- Thermal loads: air friction on the rocket and temperature increase due to engine function.
- Dynamic loads
    - Low frequency vibrations (also called sine vibrations): vibrations occurring when the engines are running
    - Random vibrations: vibrations and noise coming from the engine during lift-off and flight, mixing of the exhaust with the atmosphere air and boundary layer turbulences transferred to the spacecraft as mechanical vibrations of random nature.
    - Acoustic loads: noise coming from the engine during lift-off and flight, mixing of the exhaust with the atmosphere or the friction of air with the rocket and acting inside the cavity where the spacecraft sits, the fairing.
- Shocks: shock due to pyro devices enabling the release of the launch vehicle stages or the satellite.

In recent years, many nanosatellites have been launched into space as part of academic or governmental projects. The launch cost is reduced by utilizing the launch of a larger commercial satellite, also known as piggyback launch. Although smaller than their commercial counterparts, these satellites are subjected to similar load conditions during launch [28].

1.2 Scope of the thesis

As part of the EU-FP7 SEAM-CubeSat project, the aim of this master thesis is to help create a robust nanosatellite design which can sustain the mechanical requirements during launch when placed as secondary payload.

Chapter 2 presents the theory behind the dynamics loading conditions: random vibrations and shock spectrum. The calculation of stresses is also introduced.

Chapter 3 presents the SEAM CubeSat project.

Chapter 4 describes the launch procedure for the most-likely selected launch vehicle, the Soyuz-2-Fregat rocket. The source of the each mechanical requirement is presented and the conditions in which it applies or not for the structure of interest according to standards and the scope of this project.

Chapter 5 includes the different Finite Element simulations done on the CubeSat on its whole structure and locally. Static load, random vibrations and/or shock spectrum are simulated for each case thanks to Ansys. Stress levels are extracted when necessary and combined in order to determine safety factors.

2 Theory

In order to understand the impact of random vibration and shock on a structure, the theory behind the stress computation is presented.

2.1 Random vibration

Vibrations are a recurrent problem in engineering applications. In the case of spacecraft, random vibrations are mainly generated by the operation of the engine and the noise generated by the rocket. Nor the frequency nor the amplitude of this kind of vibration are constants, see Figure 1. Several frequencies can act on this structure at the same time.

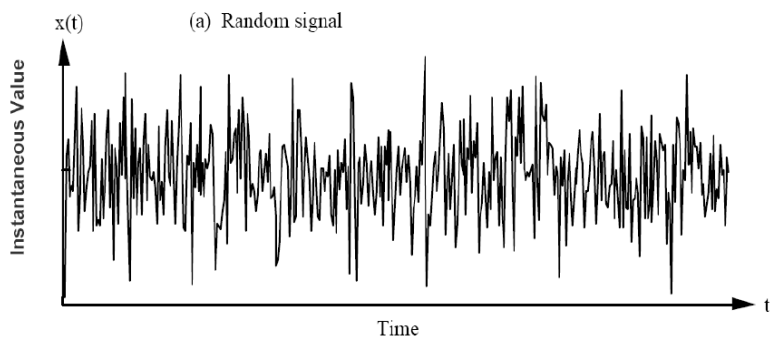

Figure 1: Random vibration [3]

Random vibrations are vibrations whose instantaneous magnitude are not specified for any given instant of time. It is therefore suitable to consider the problem in a statistical approach in order to foresee both loading - the input in the system - and the response of the structure in form of stress for example. In this case, the probability of the occurrence of a certain level of stress can be determined.

2.1.1 Mathematical tools applied to signals

In order to understand the nature of the input excitation and the resulting response of the system, some probabilistic terms and transform must be defined [7].

A process $x(t)$ is called stationary if its probability structure is independent of a shift in the time origin hence

$$p(x,t) = p(x,t+a) \tag{1}$$

A process $x(t)$ is called ergodic if its statistical properties, such as its mean and variance, can be deduced from a single, sufficiently long sample of the process.

The following definitions apply for a stationary and ergodic process.

The mean value of $x(t)$ is given by

$$\mu_x = \langle x \rangle = E(x) = \lim_{T\to\infty} \frac{1}{T} \int_0^T x(t)dt \tag{2}$$

The mean square value of $x(t)$

$$\left\langle x^2 \right\rangle = E(x^2) = \lim_{T\to\infty} \frac{1}{T}\int_0^T x^2(t)dt = \sigma_x + \mu_x \tag{3}$$

The variance of $x(t)$ is given by

$$\sigma_x^2 = E\left\{(x(t)-\mu_x)^2\right\} = E\left\{x^2\right\} - \mu_x^2 \tag{4}$$

The autocorrelation function, or auto variance function, of a stationary and ergodic random process $x(t)$ expresses the correlation of a function with itself at points separated by various times τ and is given by

$$R_{xx} = E\left\{x(t)x(t+\tau)\right\} = \lim_{T\to\infty} \frac{1}{T}\int_0^T x(t)x(t+\tau)dt \tag{5}$$

In order to convert the equation of motion in the frequency domain, the Fourier transform $X(\omega)$ for the random process $x(t)$ is given by

$$X(\omega) = \int_{-\infty}^{\infty} x(t)e^{-i\omega t}dt \tag{6}$$

A Gaussian distribution, or normal distribution, is commonly used to describe the distribution of a probability. The whole area under the probability density curve is equal to one. The probability of a value to take a certain value is described in Table 1 and shown in Figure 2.

Table 1: Probability for a random signal with normal distribution

Value taken	Percent Probability
$\mu-\sigma < x < \mu+\sigma$	68.27%
$\mu-2\sigma < x < \mu+2\sigma$	95.45%
$\mu-3\sigma < x < \mu+3\sigma$	99.73%
$\mu-4\sigma < x < \mu+4\sigma$	99.994%
$\mu-5\sigma < x < \mu+5\sigma$	99.99994%

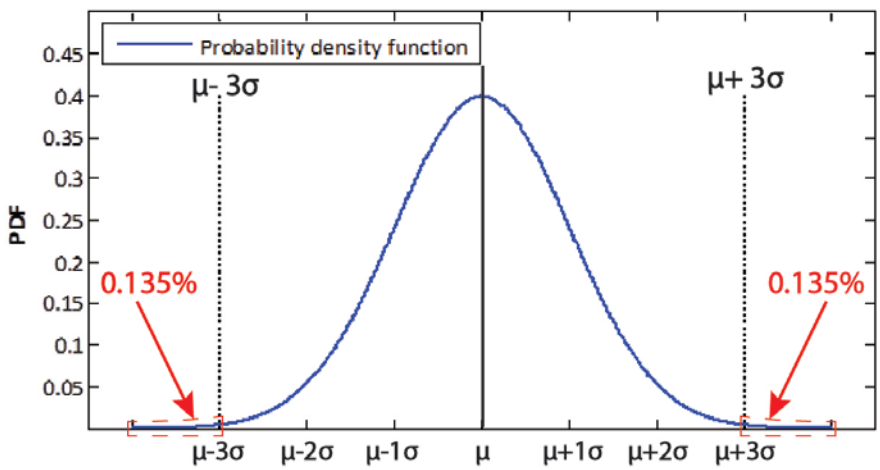

Figure 2: Gaussian distribution – Probability density functions

A 3σ analysis reflects a probability of occurrence of 99.73% and is used throughout the analysis conducted in this project.

2.1.2 Input signal: Power spectral density

The power spectral density S_{xx} (PSD) quantifies the distribution of power of the signal $x(t)$ with respect to the frequency. As the signal is a random process - acceleration, velocity or displacement for example - we cannot measure the contribution of one single frequency. The PSD indicates instead the power which is to say the quantity to which a frequency range contributes in the mean square value of the signal $x(t)$. In other words, it tells us how a certain frequency range contributes in value to the square value of the root mean square acceleration value.

The PSD is defined as the Fourier transform of the auto or cross correlation of one of two random processes. The PSD of the random process $x(t)$ is given by

$$S_{xx}(\omega) = \lim_{T\to\infty} \frac{1}{2T} \left|\mathrm{X}(\omega)\right|^2 \tag{7}$$

The actual physical power can be defined as the squared value of the signal. In practice, the PSD is expressed as a function of the frequencies in Hz and given as a one sided which is to say for positive frequencies. The one sided PSD W_{xx} is given by

$$W_{xx}(f) = 2S_{xx}(f) \tag{8}$$

Table 2 below illustrates different kinds of resulting different kinds of signal.

Table 2: Signal and corresponding PSD [9]

Type of signal		Autocorrelation		One-sided PSD	
Sine wave	$x(t) = X \sin \omega_0 t$	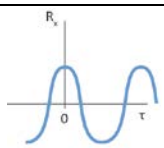	$R_{xx}(\tau) = \frac{X^2}{2}\cos(2\pi f_0 \tau)$	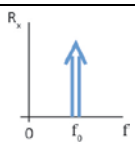	$W_{xx}(f) = \frac{X^2}{2}\delta(f - f_0)$
White noise	All frequencies excited at the same time	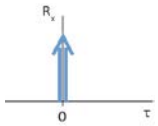	$R_{xx}(\tau) = a\delta(\tau)$	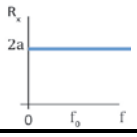	$W_{xx}(f) = 2a$

For the application at hand, the acceleration density spectrum (ASD) is of interest. The ASD used in the simulation are a result of measured acceleration during launch. The random vibration accounts for vibrations induced by the mechanical vibrations transmitted from the engine, the noise outside of the rocket generated by the engine operation or the mixing of the exhaust with ambient air. The maximum values extracted and used to create an envelope ASD which is used as a reference loading condition, see Figure 3.

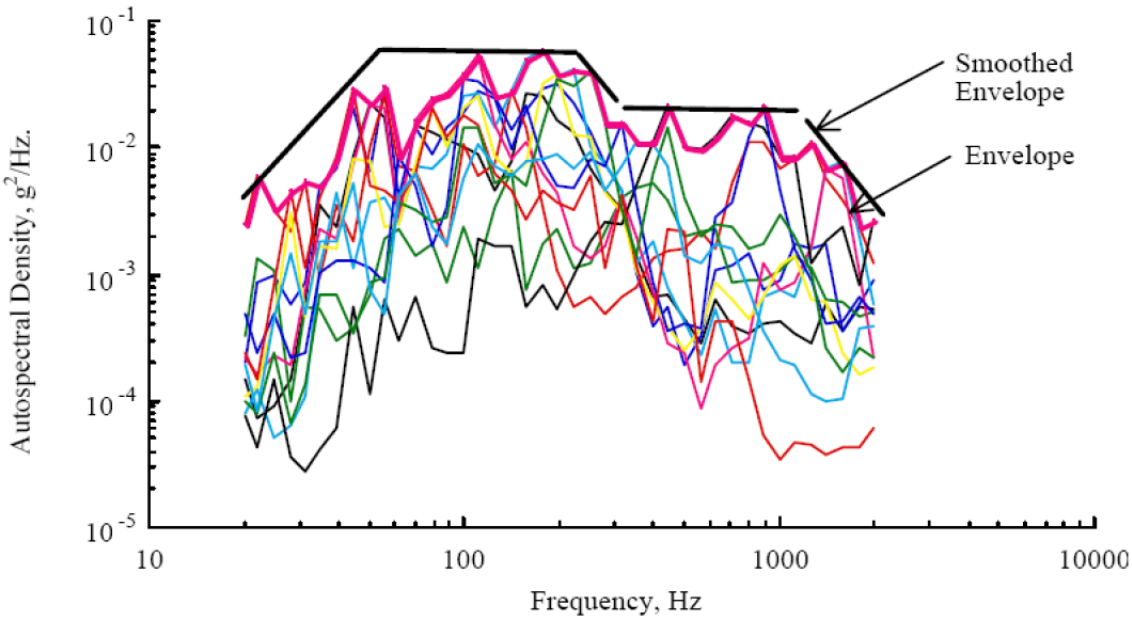

Figure 3: Creation of an acceleration density spectrum [3]

2.1.3 Mile's equation and conversion of ADS into response spectrum

Mile's equation is widely used in spacecraft application in order to calculate the response of a system subjected to vibrations [7].

The system is excited with white noise using a PSD as input, here a base acceleration given in G acceleration. The response is given in form of the root mean square (RMS) acceleration calculated in G (GRMS). The value of the GRMS is then used as a static loading on the structure in order to study upcoming stresses for example.

In order to illustrate this problem, a single degree of freedom (SDOF) system is considered where the base is excited as shown in Figure 4.

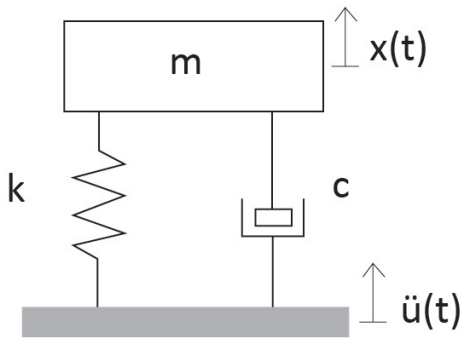

Figure 4: Base excitation on a SDOF system

The SDOF system consisting of a mass m with a damping c and a spring constant k is excited at the base with the acceleration $\ddot{u}(t)$ in form of a white noise excitation or constant PSD $W_{\ddot{u}\ddot{u}}$ where

$$W_{\ddot{u}\ddot{u}} = 2S_{\ddot{u}\ddot{u}} \tag{9}$$

The relative displacement of the mass $z(t)$ is given by

$$z(t) = x(t) - u(t) \tag{10}$$

The equation of motion for this SDOF system is given by

$$m\ddot{x}(t) + \mathrm{c}\{\dot{x} - u(t)\} + k\{x(t) - u(t)\} = 0 \tag{11}$$

The equation can be written

$$\ddot{z}(t) + 2\zeta\omega_n\dot{z}(t) + \omega_n^2 z(t) = -\ddot{u}(t) \tag{12}$$

where $\omega_n = \sqrt{\frac{k}{m}}$ is one of the eigenfrequency of the system and $\zeta = \frac{c}{2\sqrt{km}}$ the damping ratio.

The equation can be rewritten in the frequency domain using Fourier transform as

$$[-\omega^2 + 2j\zeta\omega\omega_n + \omega_n^2]Z(\omega) = -\ddot{U}(\omega) \tag{13}$$

The response function $Z(\omega)$ is then given by

$$Z(\omega) = -\ddot{U}(\omega)H(\omega) \tag{14}$$

where $H(\omega)$ is called the transfer function given by

$$H(\omega) = \frac{1}{-\omega^2 + 2j\zeta\omega\omega_n + \omega_n^2} \tag{15}$$

The power density spectrum of the response and the excitation are given by

$$S_{zz}(\omega) = \lim_{T\to\infty}\frac{1}{T}\left|\mathrm{Z}(\omega)\right|^2 \tag{16}$$

$$S_{\ddot{u}\ddot{u}}(\omega) = \lim_{T\to\infty}\frac{1}{T}\left|\ddot{U}(\omega)\right|^2 \tag{17}$$

The excitation and response PSD functions are then related by

$$S_{zz}(\omega) = \left|H(\omega)\right|^2 S_{\ddot{u}\ddot{u}}(\omega) \tag{18}$$

The autocorrelation of the PSD function $S_{zz}(\omega)$ is given by

$$R_{zz}(\tau) = \frac{1}{2\pi}\int_{-\infty}^{\infty} S_{zz}(\omega)e^{j\omega\tau}d\omega \tag{19}$$

Equation (18) is inserted into (19) and given the white noise excitation, the equation can be written

$$R_{zz}(\tau) = \frac{S_{\ddot{u}\ddot{u}}(\omega)}{2\pi}\int_{-\infty}^{\infty}\left|H(\omega)\right|^2 e^{j\omega\tau}d\omega \tag{20}$$

$\left|H(\omega)\right|^2$ can be rewritten

$$\left|H(\omega)\right|^2 = \frac{1}{\left(\omega_n^2 - \omega^2\right)^2 + \left(2\zeta\omega\omega_n\right)^2} = \frac{1}{\omega_n^4\left[\left(1-\frac{\omega^2}{\omega_n^2}\right)^2 + \left(2\zeta\frac{\omega}{\omega_n}\right)^2\right]} \tag{21}$$

The autocorrelation $R_{zz}(t)$ can now be calculated as

$$R_{zz}(\mathrm{t}) = \frac{S_{\ddot{u}\ddot{u}}(\omega)e^{-\zeta\omega_n t}}{4\zeta\omega_n^3}\left\{\cos\left(\omega_n\sqrt{1-\zeta^2}\right) + \frac{\zeta}{\sqrt{1-\zeta^2}}\sin\left(\omega_n\sqrt{1-\zeta^2}\right)\right\} \tag{22}$$

The mean square response of the relative displacement $z(t)$ by considering a white noise excitation is given by

$$E\left\{\mathrm{z}(t)^2\right\} = R_{zz}(0) = \frac{S_{\ddot{u}\ddot{u}}}{2\pi}\int_{-\infty}^{\infty}\left|H(\omega)\right|^2 d\omega = \frac{S_{\ddot{u}\ddot{u}}}{4\zeta\omega_n^3} = \frac{W_{\ddot{u}\ddot{u}}}{8\zeta(2\pi f_n)^3} \tag{23}$$

The autocorrelation functions for the velocity $\dot{z}(t)$ and the acceleration $\ddot{z}(t)$ can be calculated by differentiating the autocorrelation function of the relative displacement $z(t)$.

The mean square value for the velocity $\dot{z}(t)$ is given by

$$E\left\{\dot{z}(t)^2\right\} = R_{\dot{z}\dot{z}}(0) = \frac{S_{\ddot{u}\ddot{u}}}{2\pi}\int_{-\infty}^{\infty}(j\omega)^2\left|H(\omega)\right|^2 d\omega = \frac{S_{\ddot{u}\ddot{u}}}{4\zeta\omega_n} = \frac{W_{\ddot{u}\ddot{u}}}{8\zeta(2\pi f_n)} \tag{24}$$

And the mean square value for the acceleration $\ddot{x}(t)$ is derived with help of its autocorrelation given by

$$R_{\ddot{x}\ddot{x}}(\mathrm{t}) = (2\zeta\omega_n)^2 R_{\dot{z}\dot{z}}(\mathrm{t}) + \omega_n^4 R_{zz}(\mathrm{t}) + 2\zeta\omega_n^3 R_{\dot{z}z}(t) + 2\zeta\omega_n^3 R_{z\dot{z}}(t) \tag{25}$$

Differentiating the autocorrelation function with respect to t gives

$$\frac{dR_{xx}(\tau)}{dt} = R_{\dot{x}x}(\tau) + R_{x\dot{x}}(\tau) = 0 \tag{26}$$

Equation (25) can now be simplified and calculated for $\tau = 0$ as

$$R_{\ddot{x}\ddot{x}}(0) = (2\zeta\omega_n)^2 R_{\dot{z}\dot{z}}(0) + \omega_n^4 R_{zz}(0) \tag{27}$$

As the autocorrelation at $\tau = 0$ is equal to the mean square value (27) can be rewritten

$$E\left\{\ddot{x}(t)^2\right\} = (2\zeta\omega_n)^2 E\left\{\dot{z}(t)^2\right\} + \omega_n^4 E\left\{z(t)^2\right\} \tag{28}$$

Inserting (24)and (23) into (28) gives

$$E\left\{\ddot{x}(t)^2\right\} = \ddot{x}_{rms}^2 = \frac{\pi f_n W_{\ddot{u}\ddot{u}}}{4\zeta}(1+4\zeta^2) \tag{29}$$

In spacecraft application $0.01 < \zeta < 0.05$, therefore

$$E\left\{\ddot{x}(t)^2\right\} = \ddot{x}_{rms}^2 = \frac{\pi f_n W_{\ddot{u}\ddot{u}}}{4\zeta} = \frac{\pi}{2} f_n Q W_{\ddot{u}\ddot{u}} \tag{30}$$

where $Q = \dfrac{1}{2\zeta}$ is called the amplification factor and f_n the natural frequency.

In general, the mean value of the acceleration $\ddot{x}(t)$, $\mu_{\ddot{x}}$ is zero and therefore the variance $\sigma_{\ddot{x}}$ of the acceleration $\ddot{x}(t)$ is equal to

$$\sigma_{\ddot{x}}^2 = E\left\{\ddot{x}(t)^2\right\} - \mu_{\ddot{x}}^2 = \ddot{x}_{rms}^2 \tag{31}$$

If the PSD function of the excitation in terms of acceleration is constant in the frequency range Δf, the root mean square of RMS value of the response, the variance is given by

$$\sigma_{\ddot{x}} = \ddot{x}_{rms} = \sqrt{\frac{\pi}{2} f_n Q W_{\ddot{u}\ddot{u}}(f_n)} \tag{32}$$

Equation (32) is called the Mile's equation and is valid for a white noise excitation.

A modified version of Mile's equation taking into account the effect of multiple octave changes in the PSD input has been derived, only the final derivation is presented in the following equation for a base excitation expressed in G.

$$\ddot{x}_{GRMS} = \sqrt{\int_0^{\infty} \frac{1+(2\zeta\varphi_i)^2}{(1-\varphi_i^2)^2+(2\zeta\varphi_i)^2} \hat{U}_{APSD}(f_i) df} \tag{33}$$

where $\varphi_i = \frac{f_i}{f_n}$, $\hat{U}_{APSD}(f_i)$ is the input PDF given in G^2/Hz. The integral is replaced by a summation for numerical applications. Finally, the equivalent $\ddot{x}_{GRMS}$ is given by

$$\ddot{x}_{GRMS} = \sqrt{\sum_{i=1}^{N} \frac{1+(2\zeta\varphi_i)^2}{(1-\varphi_i^2)^2+(2\zeta\varphi_i)^2} \hat{U}_{APSD}(f_i) \Delta f_i} \tag{34}$$

This method with Mile's equation is very cost effective method but has several disadvantages [25]:

- Mile's equation is based on a SDOF and therefore cannot be used when a MDOF structure is excited in different directions at the same time.
- Mile's equation is based on a white noise excitation. If the input spectrum is rather complicated, the result from Mile's equation can include errors.
- Mile's equation is based on a SDOF where one eigenmode is predominant. The structure should respond as when equivalent acceleration is imposed onto the structure. If the predominant mode is a twisting mode, Mile's equation is not suitable.
- Mile's equation does not work in reverse which is to say that acceleration cannot be determined from Mile's equation. It only provides an estimate of the peak acceleration using the 3σ analysis.

Mile's equation is also used to convert a random vibration spectrum into a shock spectrum for design proposes. It enables a comparison of the random vibration and shock spectrums.

The converted random vibration spectrum into shock for 3σ is given by [8]

$$\ddot{x}_{3\sigma}(f_n, \zeta) = \sqrt{2\ln(f_n T)} 3\ddot{x}_{GRMS} \tag{35}$$

where T is the duration of the random vibration in seconds.

2.1.4 Stress calculation

It is important to understand what kind of results a random vibration induced stress analysis gives. The equivalent von Mises stress value given corresponds to the root mean square of the variance of the stress with a mean value equal to zero and for a probability according to a Gaussian distribution, see Table 1 and 2.1.1.

The assumption regarding the distribution of the stress probability is important to take into account. The first assumption of the analysis is that the probability distribution of the stress follows a Gaussian distribution. In reality, we do not know how the probability of the stress is distributed. The second assumption is that the mean value of the stress is equal to zero as the signal is random.

2.1.4.1 Von Mises equivalent stress for Mile's equation

Mile's equation is used to determine the GRMS response acceleration on the system. This acceleration is applied on the structure as a static load. The Von Mises Stress value is then evaluated as a result of the static load.

2.1.4.2 Von Mises Root Mean Square value for random vibration analysis

In order to assess the value of the von Mises stress in the time domain, this value should be computed for each time steps which is a very expensive method. The von Mises root mean square method, developed in [12][13], is a combination of the modal stress vectors.

We first consider the definition of von Mises stress where

$$p^2(t) = \sigma(t)^T \mathbf{A} \sigma(t) \tag{36}$$

where $\sigma(t)$ is the stress vector and $\mathbf{A}$ the von Mises stress coefficient matrix written

$$\mathbf{A} = \begin{bmatrix} 1 & -0.5 & -0.5 & & & \\ -0.5 & 1 & -0.5 & & & \\ -0.5 & -0.5 & 1 & & & \\ & & & 3 & & \\ & & & & 3 & \\ & & & & & 3 \end{bmatrix} \tag{37}$$

The stress vector is expressed with modal coordinates

$$\sigma(t) = \sum_k q_k(t) \Psi_k^\sigma \tag{38}$$

where Ψ_k^σ is the modal stress component in the point of interest for the k th mode and $q_k(t)$ is the modal coordinate at the same time t.

Inserting (38) into (36) we get

$$p^2(t) = \sum_i \sum_j q_i(t) q_j(t) \Psi_i^{\sigma} \mathbf{A} \Psi_j^{\sigma} \tag{39}$$

We are now interested in the mean square value of von Mises stress

$$E\left\{p^2(t)\right\} = \sum_{i,j} E\left\{q_i(t) q_j(t)\right\} \Psi_i^{\sigma T} \mathbf{A} \Psi_j^{\sigma} = \sum_{i,j} \Gamma_{ij} T_{ij} \tag{40}$$

where T_{ij} is called the modal stress participation factor of the mean square given by

$$T_{ij} = \Psi_i^{\sigma T} \mathbf{A} \Psi_j^{\sigma} \tag{41}$$

and Γ_{ij} is the time-lag cross-variance between the i th and the j th modal coordinates.

$$\Gamma_{ij} = E\left\{q_i(t) q_j(t)\right\} \tag{42}$$

Γ is a modal quantity whereas T varies with the modal stress component for each location. Γ is estimated according to [6] as

$$\Gamma = \frac{1}{2\pi} \int_{-\infty}^{\infty} \overline{H(\omega)} S_{ff}(\omega) H(\omega)^T d\omega \tag{43}$$

where $H(\omega)$ is the modal transfer function between the modal coordinate and the input force and $\overline{H(\omega)}$ is the complex conjunction form, $S_{ff}(\omega)$ represents the cross spectral density of the input force.

The modal transfer function for the modal coordinate k due to an input force for the degree of freedom a can be written as:

$$H_{ka}(\omega) = \frac{1}{\omega_k^2 - \omega^2 + 2 j \zeta_k \omega \omega_k} = \varphi_{ak} D_k(\omega) \tag{44}$$

here φ_{ak} is the component of the displacement eigenvector, for a given mode k, corresponding to the degree of freedom a, ω_k and ζ_k respectively the modal frequency and modal damping for that mode.

Inserting (44) into (43) we get

$$\Gamma_{ij} = \sum_{a}^{N_f} \sum_{b}^{N_f} \varphi_{ai} \varphi_{bj} \left[\frac{1}{\pi} \int_0^{\infty} \mathrm{Re}\left(\overline{D_i(\omega)} D_j(\omega) \left[S_{ff}(\omega) \right]_{ab} \right) d\omega \right] \tag{45}$$

In numerical application this integral can be approximated by the following summation in the frequency domain

$$\Gamma_{ij} = \sum_{a}^{N_f} \sum_{b}^{N_f} \varphi_{ai} \varphi_{bj} \left[\sum_{n=1}^{N_\omega} \mathrm{Re}\left(\overline{D_i(2\pi f_n)} D_j(2\pi f_n) \left[S_{ff}(2\pi f_n) \right]_{ab} \right) \Delta f \right] \tag{46}$$

where N_f is the number of direction excited and N_f is the number of discretization in frequency for the sum.

2.2 Shock response spectrum

Shock occurs when a launch vehicle or satellites separates from the launch vehicle. These shocks are due to pyrotechnic devices developed to enables a part to be released from the main vehicle. The satellite is therefore subjected to strong accelerations rapidly decaying with time, see Figure 5. The acceleration given in the time domain is then converted into a shock response spectrum.

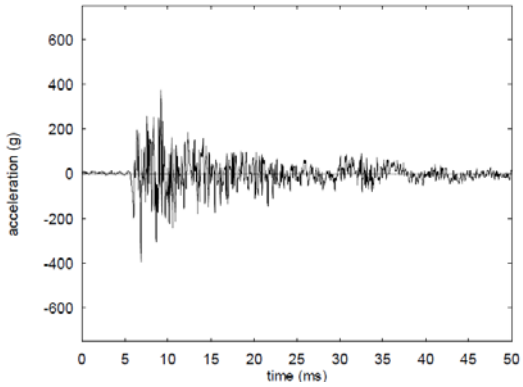

Figure 5: Typical acceleration during booster's separation [3]

2.2.1 Definition

The shock response spectrum (SRS) is broadly defined as the peak response of a simple oscillator (single degree-of-freedom system) to an excitation as a function of the natural frequency of the oscillator [17]. In other words, the response spectrum shows how the system responds at each frequency to a certain excitation as if the system reacted independently for each frequency. As opposed to a random process, the response spectrum is not probabilistic. The shock response spectrum gives the peak response of each SDOF system with respect to the natural frequency for a given constant damping ratio, see Figure 6.

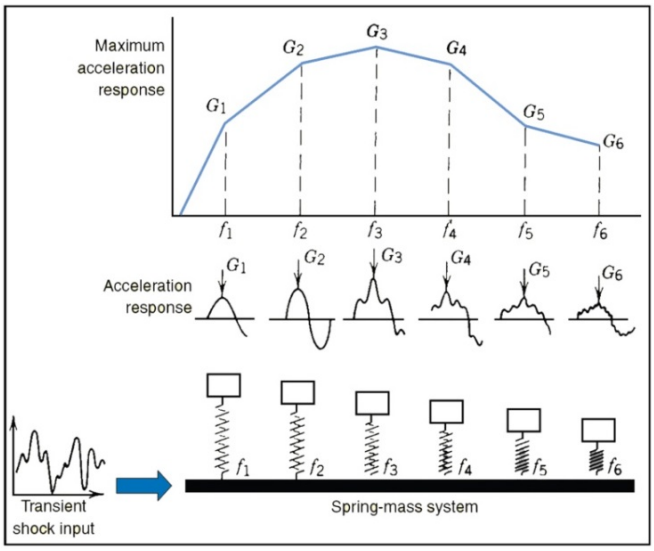

Figure 6: How a response spectrum is developed [18]

A SDOF non-damped system is excited at its base excited; the equation of motion is given by [17].

$$m\ddot{x}(t) + k\left\{x(t) - u(t)\right\} = 0 \tag{47}$$

The relative displacement of the mass $z(t)$ is given by

$$z(t) = x(t) - u(t) \tag{48}$$

The equation can be written

$$\ddot{z}(t) + \omega_n^2 z(t) = -\ddot{u}(t) \tag{49}$$

where ω_n is the Eigen frequency of the system. Inserting (48) into (47), the absolute acceleration of the mass is then written

$$\ddot{x}(t) = -\omega_n^2 z(t) \tag{50}$$

Duhamel's integral is used to solve (49) which gives

$$z(t) = -\frac{1}{\omega_n}\int_0^t \ddot{u}(\tau)\sin\omega_n(t-\tau)d\tau \tag{51}$$

The absolute acceleration can be now written

$$\ddot{x}(t) = \omega_n\int_0^t \ddot{u}(\tau)\sin\omega(t-\tau)d\tau \tag{52}$$

The shock response is defined as the maximum $\left|\ddot{x}(t)\right|$ for each frequency

$$S_A \equiv \left|\ddot{x}(t)\right|_{\max} \tag{53}$$

The shock response spectrum for a non-damped system is now given by

$$S_A = \left|\omega_n\int_0^t \ddot{u}(\tau)\sin\omega(t-\tau)d\tau\right|_{\max} \tag{54}$$

When damping is included, the shock response spectrum is given by

$$S_A = \left|\omega_n\int_0^t \ddot{u}(\tau)e^{-\zeta\omega(t-\tau)}\sin\omega(t-\tau)d\tau\right|_{\max} \tag{55}$$

2.2.2 Stress calculation

The equivalent stress for the response spectrum analysis is calculated thanks to the combination of modal stress vectors [19][20]. First a modal analysis is performed and modal stress components ψ_i^a are extracted for each point and degree of freedom. The stress values represent the stress found for the maximum positive amplitude of the mode. The modal stress component ψ_i^a is scaled by the mode coefficient A_i given by

$$A_i = \frac{S_{ai}\gamma_i}{\omega_i^2} \tag{56}$$

where ω_i is the modal frequency, S_{ai} is spectral acceleration for the i th mode, obtained from the input acceleration response spectrum at frequency f_i and effective modal damping ratio ζ_i, and γ_i is the participation factor given by

$$\gamma_i = \varphi_i^T \mathbf{MD} \tag{57}$$

where φ_i is the normalized eigenvector, $\mathbf{M}$ is the modal mass matrix and $\mathbf{D}$ is the vector describing the excitation direction which derivation can be found in [12].

The stress components are combined using the Square Root of the Sum of the Squares (SRSS) Method and final stress component for each degree of freedom at each point σ_i^a is given by

$$\sigma_i^a = \sqrt{\sum_{i=1}^{N}\left(A_i\psi_i^a\right)^2} \tag{58}$$

The von Mises stress is then computed as per its definition taken into account the different DOF at each point.

3 Background on the SEAM Cube Sat project

Micro- and nanosatellites have become a valuable tool for space research due to their relatively low development and launch costs. The CubeSat standard has been introduced to create a standard for the launching system. The satellites have a standard dimension of 100x100x100 mm^3 as 1U standard, or a multiple of those – e.g. 300x100x100 mm^3 for a 3 unit CubeSat. A considerable number of CubeSats have been launched, the majority of them being demonstration or educational missions.

The SEAM project aims to develop an electromagnetically clean nanosatellite to acquire high resolution data about the ionosphere magnetic field [15]. The SEAM CubeSat is a 3 unit CubeSat with deployable booms equipped with sensors, see Figure 7 and Figure 8.

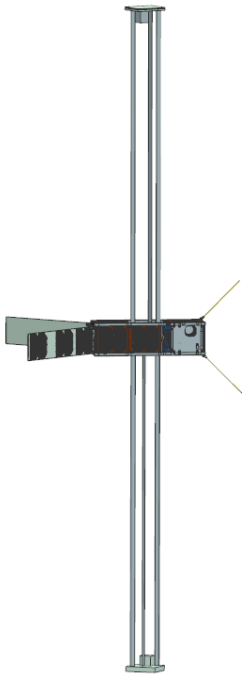

Figure 7: Deployed SEAM CubeSat

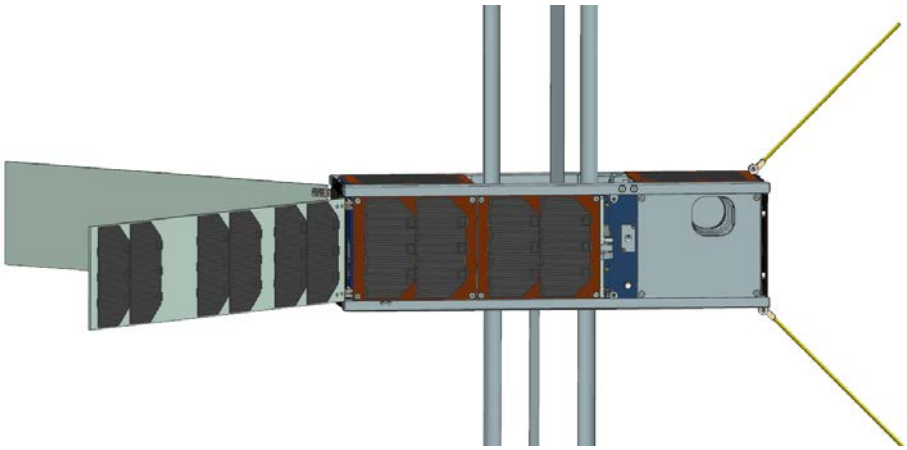

Figure 8: Close view of the deployed SEAM CubeSat

SEAM is a collaborative project aiming at developing, building, launching and operating a nanosatellite for science-grade measurements of magnetic field of the Earth. The consortium brings together eight partners from five European countries: KTH, ÅAC Microtec, ECM Space Technologies, LEMI, BL Electronics, GomSpace, The Swedish Space Corporation (SSC) and Kayser Italia.

A CubeSat is launched as a secondary payload by placing a CubeSat dispenser, also called Poly-Pico Satellite Orbital Deployer (P-POD), see Figure 9. This devise ejects the CubeSat thanks to a spring loaded plate. The P-POD is placed inside the fairing under the main satellite, as presented in the next chapter.

Figure 9: CubeSat dispenser also called P-POD

4 Launch steps, load combinations and safety factor

4.1 Launch steps

A rocket can host several satellites, also called payloads; the main satellite, called the first payload, and one or several smaller satellites also called secondary or auxiliary payloads. The first payload can for instance be a commercial satellite. Nanosatellites are usually secondary payloads which take advantage of a launch opportunity therefore reducing launch costs. As shown in Figure 10, the secondary payloads are placed under the first payload and are released last, as described in Table 3. Therefore, the influence of the first payload release on the secondary payload is to be taken into account.

At this point in the SEAM project, the launch rocket is not known with certainty. However, the Soyuz-2-Fregat rocket has been determined to be the most likely choice and therefore will be the reference in this report [16].

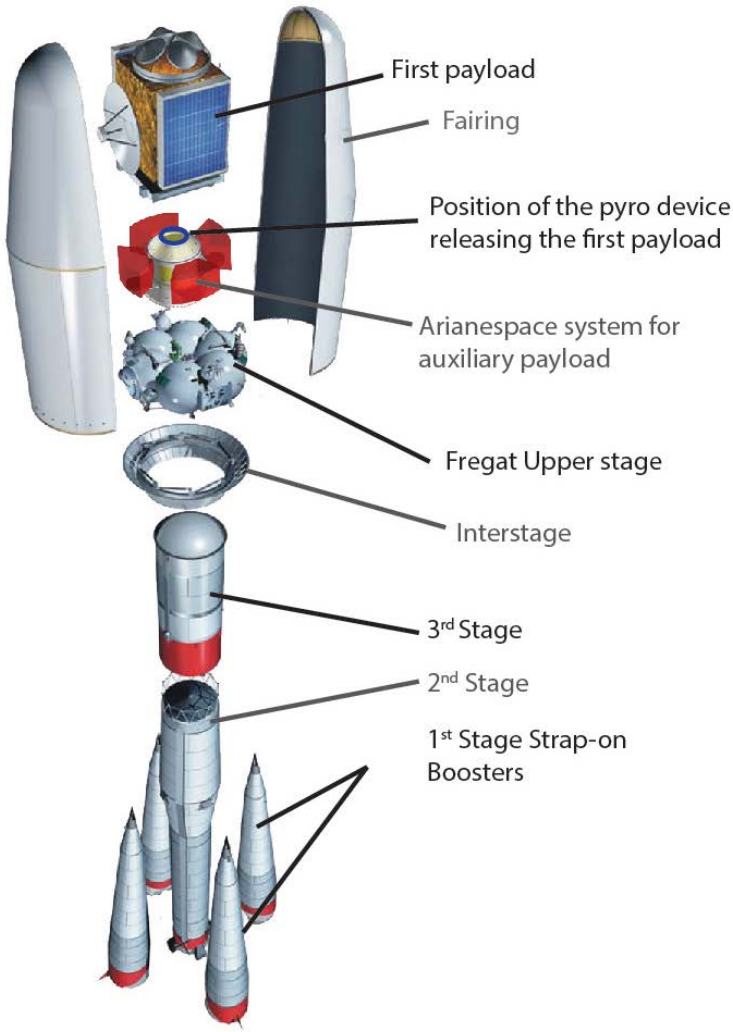

Figure 10: Soyuz rocket detailed model with secondary/auxiliary payload adapter, [2].

Table 3: Launch steps for the Soyuz-2-Fregat rocket [1]

Launch step	Description
Step 1	The engines ignite and liftoff occurs.
Step 2	The first stage solid rocket boosters burn off their fuel and separate from the rocket. Boosters burn off fuel and jettison which is to say they are released from the rocket. The second stage or engine is revealed. The second stage ignites and pushes the rocket farther along its path.
Step 3	The fairing jettisons when the rocket has passed a certain altitude where the air friction thermal loading on the fairing is about the same as the Sun's heating effect.
Step 4	The second stage burns off fuel and jettisons. The third stage engines push the rocket further away.
Step 5	The third stage is released.
Step 6	The Fregat engines start in order to place the spacecraft into orbit.
Step 7	The first payload separates from the rocket and begins its mission in space.
Step 8	The secondary payloads are released into space. A CubeSat slides out of its dispenser when pushed out by a spring loaded plate.

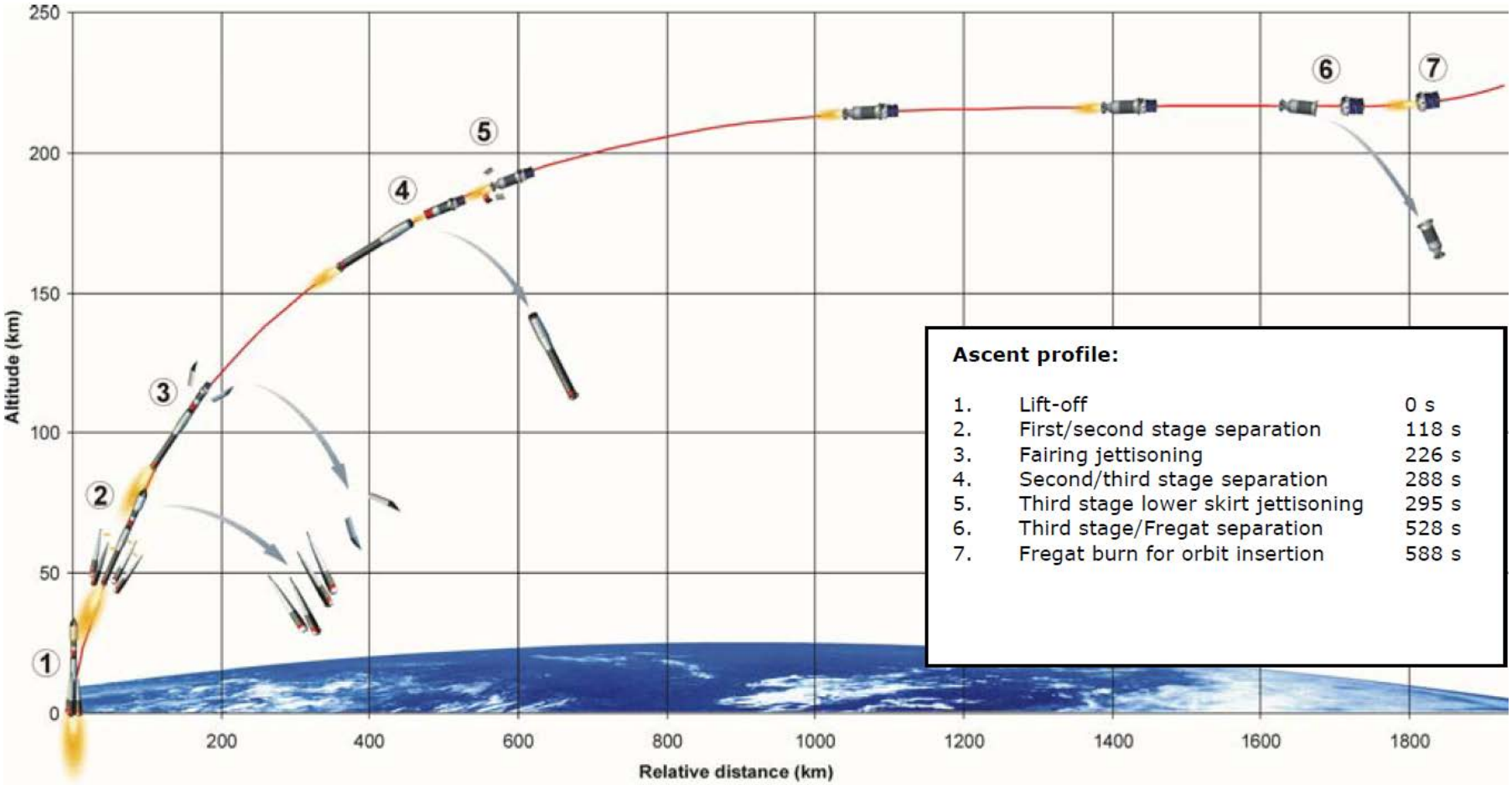

Figure 11: Typical ascent profile for Soyuz [1]

4.2 Mechanical environment

Each of the launch stages is associated with a mechanical loading condition. Thermal loads are not treated in this report. The sequence of these loading conditions is summarized in Table 4.

The payload is subjected to a quasi-static acceleration due to the acceleration of the rocket during ascent. The vibrations of the engine of the different stages are mechanically transferred to the payload in form of low frequency sine vibrations and random vibrations. The mixing of the exhaust with the atmosphere is a source of noise that excites the vibration of the fairing which in turn is transmitted to the payload. In the same way aerodynamic sources, such as wind, turbulence and air friction generates noise and vibrations transmitted as random vibration to the payload. Inside the fairing, sound pressure generated by all the source of noise acts directly onto the payload. Pyro devises are used to separate the launch vehicle stages, the fairing or the payloads from the rocket exposing the payload to shocks.

Table 4: Loading conditions spectra provided by the launch operator and their occurrence during flight stages and separation steps.

<table>
<tr><th>Loading condition</th><th>Quasi-Static loading</th><th>Sine vibration (SV)</th><th>Random vibration (RV)</th><th>Acoustic load*</th><th>Shock</th></tr>
<tr><td>Source / Launch steps</td><td>Acceleration of the rocket</td><td>Engine operation</td><td>Engine vibration and noise, air friction</td><td>Engine, air friction, etc.</td><td>Pyro devises used to separate launch vehicles or satellite</td></tr>
<tr><td>Lift-off</td><td rowspan="6">Maximum longitudinal and lateral accelerations</td><td rowspan="6">SV levels for operation of launch vehicle stages</td><td rowspan="2">RV for 1st stage flight</td><td rowspan="4">Sound pressure level spectrum</td><td></td></tr>
<tr><td>1st stage flight</td><td></td></tr>
<tr><td>1st stage separation</td><td rowspan="3">RV for 2nd and 3rd stage flight</td><td>1st stage SRS**</td></tr>
<tr><td>2nd stage flight</td><td></td></tr>
<tr><td>Fairing separation</td><td rowspan="9"></td><td>Fairing SRS**</td></tr>
<tr><td>2nd stage separation</td><td>2nd stage SRS**</td></tr>
<tr><td>3rd stage flight</td><td rowspan="8"></td><td rowspan="2"></td><td rowspan="2"></td><td></td></tr>
<tr><td>3rd stage separation</td><td>SV levels for Fregat flight</td><td>RV for Fregat flight</td><td>3rd stage SRS**</td></tr>
<tr><td>Fregat flight</td><td></td></tr>
<tr><td>Fregat separation</td><td rowspan="3"></td><td rowspan="3"></td><td>Upper stage SRS**</td></tr>
<tr><td>1st payload release</td><td>First payload SRS**</td></tr>
<tr><td>2nd payload release</td><td></td></tr>
</table>

***applied directly onto the spacecraft when inside the fairing**

**** SRS: Separation shock response spectrum**

4.3 Test/simulation requirements

Satellite development projects require years of preparation. In the first stage of the development, it is crucial to dimension the spacecraft with sufficient safety margin to sustain loading conditions in the toughest of launch environments. The structure of interest in this project is a secondary payload.

Previous knowledge is available to the development engineers in form of standards such as NASA's [4][5]. Another source of information is provided by the actual launch provider [1]. As piggyback launches are not the primarily source of income for launchers, most information regarding spectra concerns those affecting the first payload. However, some launch providers such as Spaceflight [6] are now offering to facilitate the launch of secondary payload and provide test guidelines specifically targeted for this kind of payload. All the different test guidelines have here been considered to find the suitable test environment for our project.

In order to design a robust spacecraft, the load contribution of each launch step must be identified and whether or not the secondary payload is affected. Appropriate load combinations are then considered.

4.3.1 Sine vibration

Sine vibrations can be excluded test if the lowest natural frequency of the spacecraft is higher than 40 Hz [16]. In the projects of interest, the two studied structures meet this requirement; therefore no sine vibration simulation has been carried out.

4.3.2 Acoustic load

Acoustic loads inside of the fairing have an impact on large thin panels such as large solar panels [7]. The two studied structures do not include such elements and therefore acoustics loads have also been discarded from this study.

4.3.3 Quasi-static load

Acceleration values are given for the maximum value during ascent. The acceleration varies during the different stages as shown in Figure 12.

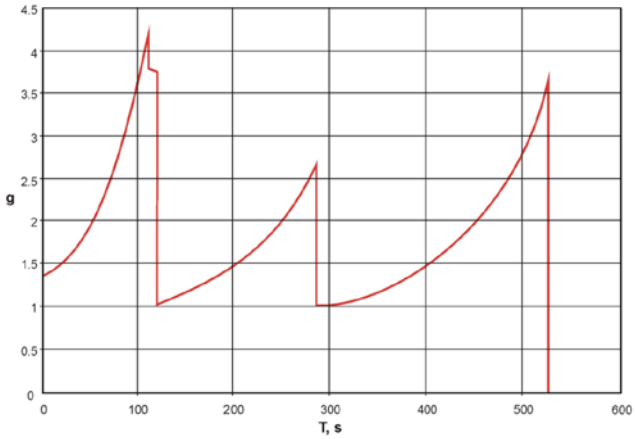

Figure 12: Typical longitudinal acceleration Soyuz rocket [1]

The maximum longitudinal and lateral accelerations have been compared between the different available sources, see Table 5.

Table 5: Maximum acceleration values given by different source

	Longitudinal acceleration [G]	**Lateral acceleration [G]**
Mission environment [16]	**10**	**5**
Soyuz user manual [1]	4.3	0.4

In order to ensure that the analysis is conservative, the higher acceleration values from the Mission environment are to be applied on the structures. The positioning of the satellites in the rocket is yet to be confirmed and therefore, the orientation generating highest stress values in the secondary payload is assumed.

4.3.4 Random vibration

The different random vibration spectra are compared between the different flight stages and for different sources [1][4][16], see Figure 13. The NASA acceleration density spectrum is selected as random vibration spectrum and will be used in the simulations as specified by the NASA test requirement.

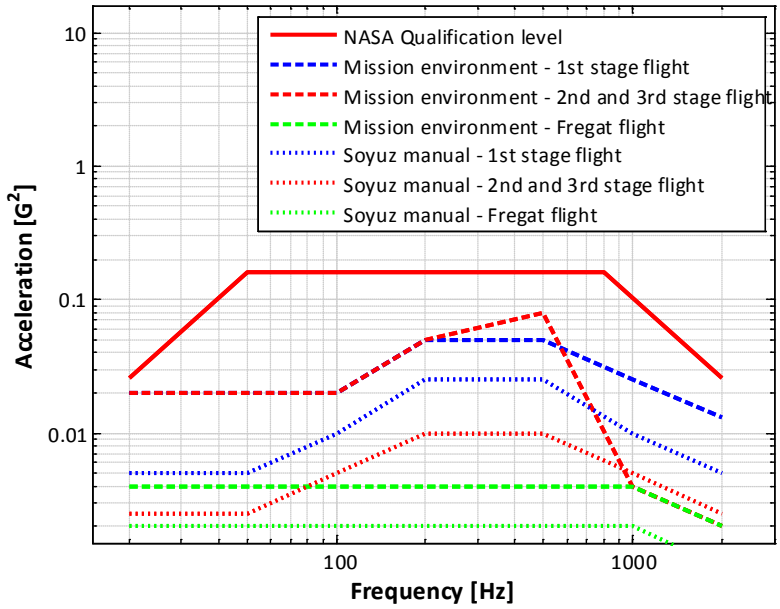

Figure 13: Comparison between Mission environment Soyuz manual and NASA Qualification ASD spectra for random vibration

4.3.5 Shock

Several shocks occur during launch. The first shocks are generated by the rocket stages jettisoning one after the other. The separation of the fairing during the 3rd stage flight is another source of shock. The final shock occurs when the first payload is released. The release of the secondary payload itself is usually of not critical and therefore rarely considered. A CubeSat for example will slide of its dispenser with a moderate velocity.

Different shock spectrum sources have been compared. The Soyuz User Manual (UM) [1] and Mission environment document [16].

In order to identify the applicable shock spectrum in further simulations, the NASA test requirement for CubeSat is first examined [5]. This standard states the following:

"Shock testing is not required when the following conditions are met:

> Condition 1: The qualification random vibration test spectrum when converted to an equivalent shock response spectrum (3-sigma response for Q=10) exceeds the qualification shock spectrum requirement at all frequencies below 2000 Hz.
>
> Condition 2: The maximum expected shock spectrum above 2000 Hz does not exceed (g) values equal to 0.8 times the frequency in Hz at all frequencies above 2000 Hz, corresponding to the velocity of (50 inches/second)."

The two conditions are reviewed by comparing the NASA Qualification random vibration spectrum, converted into shock spectrum with (35), with the different shock spectra referring to different shock instances or given by different sources [1][4][6][16].

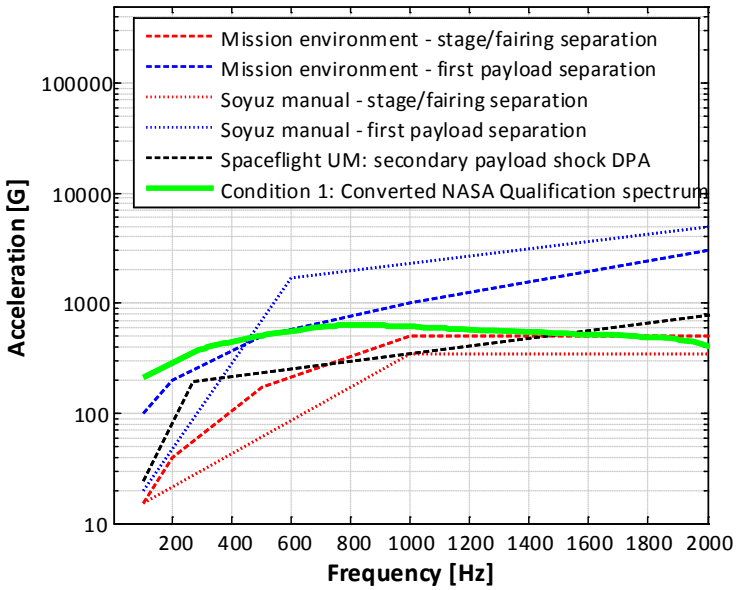

Figure 14: Condition 1 for frequencies below 2000 Hz

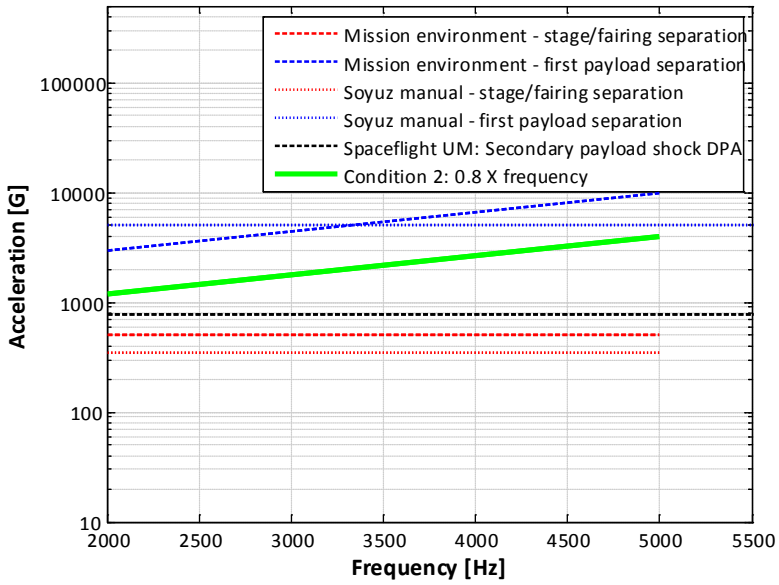

Figure 15: Condition 2 for frequencies above 2000 Hz

The analysis concludes the following:

- The Fairing/separation shock spectrum does not need to be included in testing as the converted NASA Qualification random vibration spectrum exceeds it in value.
- The second payload will be tested for shock against the separation of the first payload using the Spaceflight secondary payload DPA spectrum which gives the shock spectrum for the side plate of the CubeSat dispenser, see Table 6.

Table 6: Shock spectrum for 1st payload shock separation transmitted the P-POD side plate [6]

Frequency [Hz]	Acceleration [g]
100	24
270	195
2000	775
10000	775

4.3.6 Load combination

After reviewing the different test requirements, two load cases are to be simulated for the CubeSat structure, see Table 7.

Table 7: Load combination and load values

	Load designation and value	
Load case 1	Random vibration	NASA Qualification level
	Acceleration	Longitudinal 10G Lateral 5G
Load case 2	Shock	Spaceflight Shock from 1st payload measured on side of P-POD

For load case 1, the total value of the stress $\sigma_{VMtot,\mathrm{i}}$ used to calculate the safety factor is the sum of the stresses is then given by

$$\sigma_{VMtot,1} = \sigma_{3\sigma VM,RV} + \sigma_{VM,Static} \tag{59}$$

It is important to note that the RMS value extracted from the random vibration analysis $\sigma_{3\sigma VM,RV}$ is given for a 3σ analysis and of probabilistic nature, whereas stress from static loading $\sigma_{VM,Static}$ is deterministic. The addition of the static loading is shifting the mean stress value.

For load case 2, only the von Mises stress values from the shock response spectrum simulation $\sigma_{VM,SRS}$ are taken into account and therefore the stress used to calculate the safety factor is

$$\sigma_{VMtot,2} = \sigma_{VM,SRS} \tag{60}$$

4.4 Safety factor

To assess the robustness of the design, safety factors are calculated from the simulations. The minimum required value is first to be determined. The calculation of the safety factor against yielding is then presented.

4.4.1 Determination of the minimum required safety factor

The determination of an appropriate safety factor is a delicate matter requiring strong engineering experience. However, standards such as the one created by the European Cooperation for Space Standardization states that several factors should be taken into account [21]. For the current project, the following factors have been considered:

- Modelling factor K_M to account for inaccuracies in the mathematical/FEM models
- Material factor K_{MT} to account for discrepancy in material parameter values
- Load factor K_L to account for inaccuracy in the load determination

The minimum safety factor for the structure is then given by

$$\eta_{Min} = K_M \cdot K_{MT} \cdot K_L \tag{61}$$

ECSS standard values were used to determine the modelling and material factors [21] and presented in Table 8.

Table 8: Partial and minimum safety factors

Factor	Value
Modelling factor	1.25
Material factor	1.25
Load factor	1
Minimum safety factor	1.56

As presented in 4.3, the load values and spectra chosen for the simulations are the most conservative. The random vibration spectrum chosen is the NASA Qualification level. Its GRMS values are higher by a factor 6.4 compared to the values of the highest spectrum of the Soyuz manual, and a factor 2 compared to the Mission environment description values, see Figure 13. The maximum quasi static acceleration values are from the Mission environment is higher by a factor 2 compared to the Soyuz manual values, see Table 5. Therefore, the load factor is set to 1.

4.4.2 Safety factor against yielding

4.4.2.1 Deterministic approach

The main interest in this project is to determine if a given structure can sustain a certain loading condition. In order for the structure to remain undeformed after launch, no plastic deformation should occur and therefore the maximum value of the von Mises stress extracted from the different simulations should be under the yield strength of the material σ_y with a certain margin.

The safety factor against yielding is then given by,

$$\eta_y = \frac{\sigma_y}{\sigma_{VMtot,i}} \tag{62}$$

where $\sigma_{VMtot,i}$ is the total von Mises stress value given by (59) for load case 1 consisting of the 3σ random vibration and static analysis and by (60) for load case 2 consisting of the shock response spectrum analysis.

4.4.2.2 Probabilistic approach

Given that the stress value given for the random vibration analysis is of probabilistic nature, the probability for the initiation of plastic deformation could be considered instead of the safety factor named before for load case 1.

The total stress value is given by (59). If the total stress is equal to the yield strength of the material then

$$\sigma_y = x\sigma_{1\sigma VM,RV} + \sigma_{VM,Static} \tag{63}$$

The number of standard deviation x required to reach the yield strength and given by

$$x = \frac{\sigma_y + \sigma_{VM,Static}}{\sigma_{1\sigma VM,RV}} \tag{64}$$

5 Simulations

The SEAM CubeSat is a three unit cube. The first cube includes circuit boards, the second consists of the deployable boom assembly with magnetic sensors and the third includes the star tracker part of the navigation system of this satellite, see Figure 17.

The CubeSat is a complex structure with numerous parts. It constitutes of an aluminum structure filled with a number of circuit boards and covered with solar panels, see Figure 17. These last items mainly consist of rigid glass-reinforced epoxy laminate (FR4) covered with electronic components, see Figure 16. The boom placed in the middle of the structure includes plates deployed thanks to glass fiber arms behaving like a self-retracting tape measure.

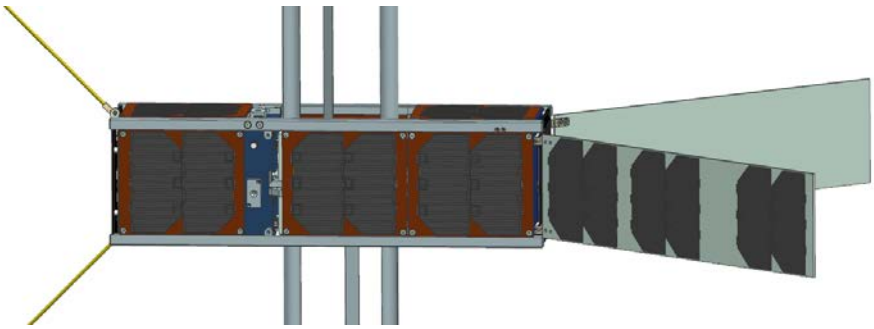

Figure 16: CubeSat with deployed solar panels on the right hand side, deployed antennas on the left hand side and part of deployed booms in the middle.

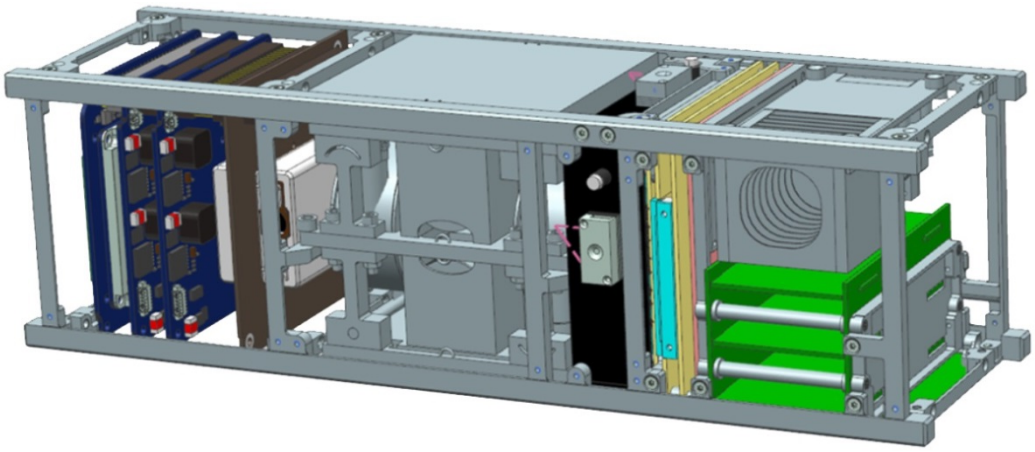

Figure 17: Inside view of the CubeSat components – boom assembly in the middle and star tracker on the right end side.

The CubeSat's geometry is first simplified. Some components such as the deployable solar panels and the deployable antennas shown in see Figure 16 are excluded from the study. The entire structure is then studied as one entity and in details in order to determine if the design can sustain the two load cases presented in 4.3.6. All simulations are conducted in the software Ansys 15.0.

5.1 CubeSat structure

The CubeSat consists of standard or "off the shelf" and custom design parts. Its structure, and particularly its aluminum frame, has been of interest in this study. The design and material have been changed throughout the iterative design process. Only results for the final design are presented here.

5.1.1 Model

The complex CubeSat structure is modeled in order to simulate the two load cases. This analysis is linear.

5.1.1.1 Geometry and material

The different part names and their linear elastic material parameters are presented in Table 9, Figure 18, Figure 19 and Figure 20. The global coordinate system can be seen in these figures.

The aluminum structure geometry is kept in its original shape in order to make sure that the stiffness of the aluminum structure is as close to reality as possible. However, screw assemblies are excluded, and replaced by bounded contact between the parts, except for the fours bolts attaching the boom frame to the ladder.

The solar panels have been modelled as simple plates made of FR4 as to provide additional stiffness and reflect accurate mass distribution. In order to include all mass, the density of the plates has been increased to reflect the presence of electronic components and adjusted in accordance to their actual mass. However these items are not of primary interest in this study.

Table 9: Material properties

Item	Item color in figures	Material	Elastic Modulus [GPa]	Poisson's ratio	Tensile strength [MPa]	Ultimate strength [MPa]	Density [kg/m^3]
Ladder	Green	AL7075-T6	70	0.33	510	590	2810
Ribs	Purple	AL7075-T6	70	0.33	510	590	2810
Ribs	Purple	AL7075-T6	70	0.33	510	590	2810
Aluminum plates	Purple	AL7075-T6	70	0.33	510	590	2810
Boom supporting frame	Grey	AL7075-T6	70	0.33	510	590	2810
Boom frame screws		Titanium alloy	96	0.36	880	950	4620
Solar panels 1.1 mm	Red	FR4CW	23.4	0.14	65	310	3800*
Solar panels 1.8 mm	Blue	FR4CW	23.4	0.14	65	310	4200*
PCB Stack	Orange	FR4CW	23.4	0.14	65	310	10500*

*Different densities reflecting the additional weight of electronic components mounted on the plates

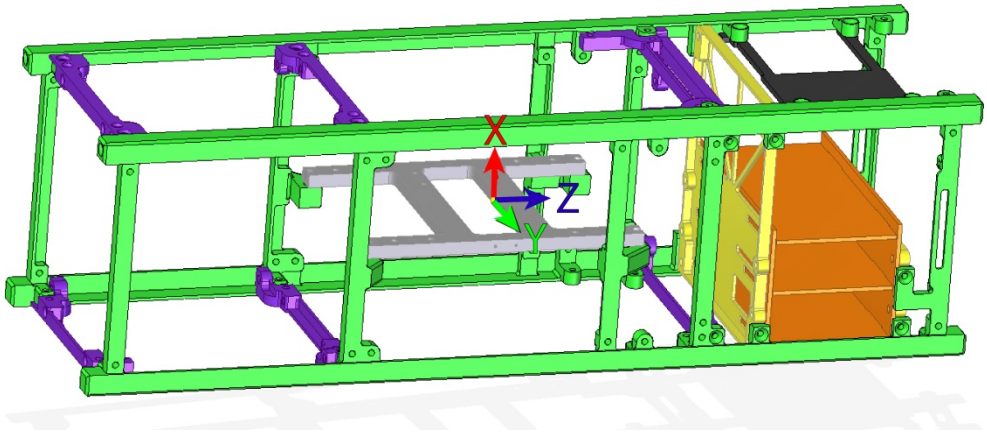

Figure 18: Modeled structure without solar panels

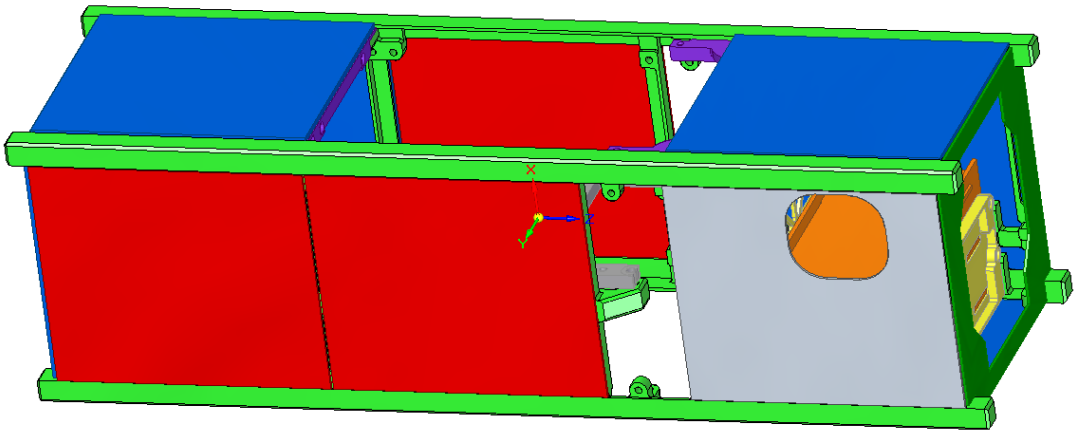

Figure 19: Modeled structure with solar panels, view A

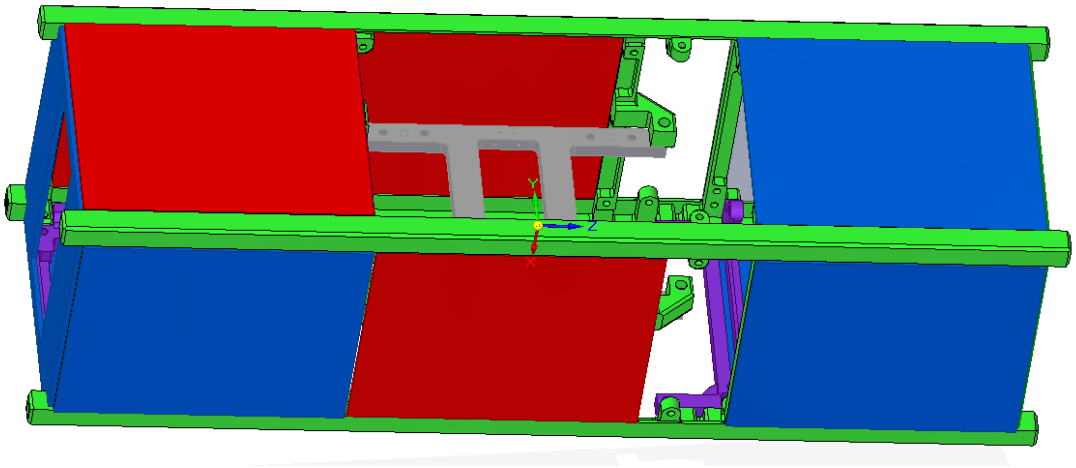

Figure 20: Modeled structure with solar panels, view B

5.1.1.2 Mass point

In order to account for the mass of the components not modelled, i.e. non-structural mass, such as circuit boards, boom and star tracker, point masses are added, see Figure 21.

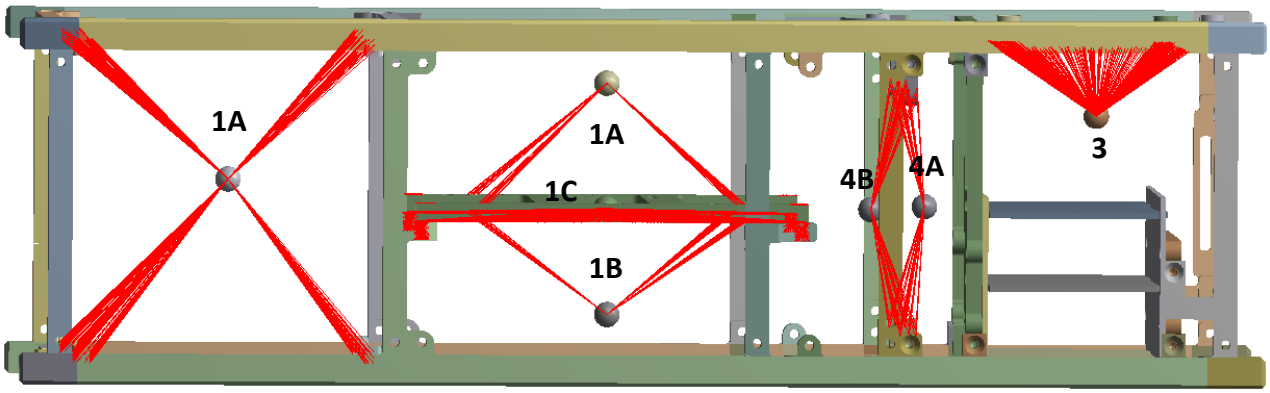

Figure 21: Modelled point masses

The coordinate, mass and moment of inertia are determined from the actual mass and geometry of the complete system, see Table 10.

Table 10: Point masses parameters

Point Mass #	Part Mass	Position coordinate [mm]			Moment of inertia [kg/m^2]		
	[kg]	X	Y	Z	Ixx	Iyy	Izz
1A	0.350	31.184	-0.214	-8.000	4.32E-04	6.35E-04	6.16E-04
1B	0.347	-32.002	-0.505	-7.668	3.68E-04	6.05E-04	5.92E-04
1C	0.098	-3.039	-0.392	-8.008	1.67E-04	1.50E-04	4.70E-05
2	0.777	4.646	-0.446	-111.411	8.75E-03	8.84E-03	7.34E-04
3	0.159	22.878	6.535	125.536	2.65E-03	2.65E-03	2.27E-04
4A	0.197	-2.359	-3.887	79.119	1.37E-03	1.37E-03	2.70E-04
4B	0.228	-2.993	0.356	64.310	1.06E-03	1.05E-03	2.12E-04

The point masses are linked to the structure by constraint equation. These links are rigid which might overconstrain the model. However, the sub systems could not be tested prior to this study, therefore the actual stiffness of theses blocks was unknown and this approach was chosen.

5.1.1.3 Meshing and contact

The structure is meshed in order to reduce the number of nodes in non-sensitive areas and increase the mesh quality in the region of interest, see Figure 22 and Figure 23. The volumes have been divided if necessary to facilitate meshing.

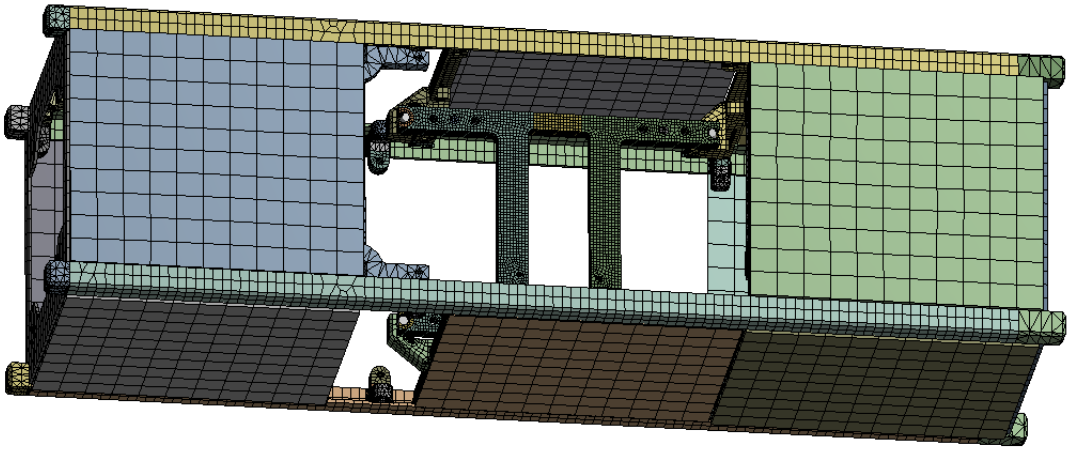

Figure 22: Mesh including solar panels

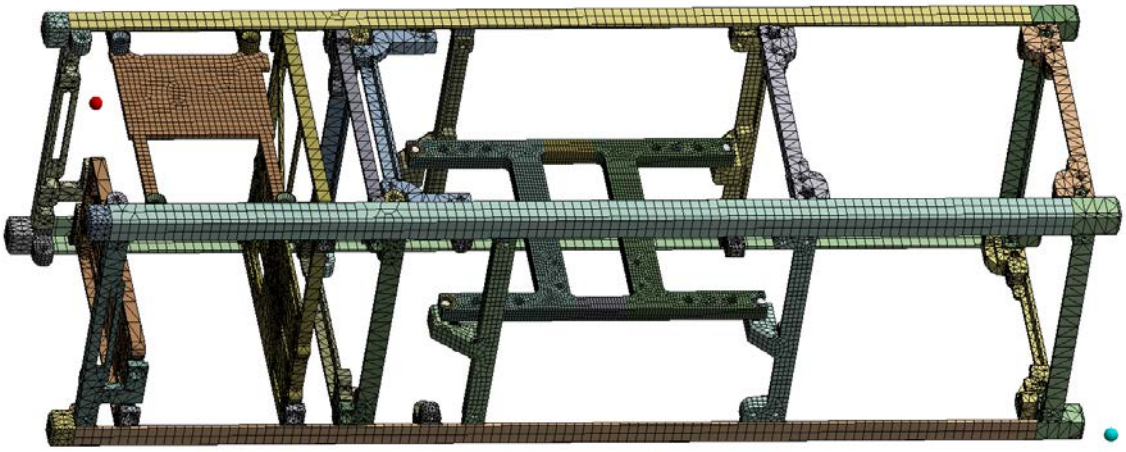

Figure 23: Mesh excluding solar panels

Due to the limitation of the allowed number of nodes for the used version of the software, the focus has been placed on the sensitive custom design areas. The quality of the mesh for certain items such as the ribs could be improved with better computing possibilities. However, these components are “off the shelf” design and therefore have been used in previous CubeSat launch and therefore known as non-sensitive components.

The structure has been meshed with different element types listed in Table 26.

Table 11: Meshing parameters

Element name	Shape	Number of nodes per element	Degree of freedom per node	Structural components meshed with element type
SOLSH190	Hexahedral	4	3	Thin panels: Solar panels
SOLID185	Hexahedral	8	3	Ladder Rails, boom, star tracker plate
SOLID 186	Hexahedral	20	3	Ladder “Ears”
SOLID187	Pyramidal	10	3	Ribs, aluminum plates
MASS21		1	6	Point masses
BEAM188		2	6	Mass links
TARGE170		N/A	N/A	All bounded contacts
CONTA174		N/A	N/A	

The analysis is linear and therefore all contacts are no slip/ bounded contacts.

The supporting frame and the “ladder ears” are of particular interest. Therefore, the mesh has been refined in this area. Furthermore, the supporting frame is attached with titanium alloy screws to the ladder “ears”. These screws have been modelled as beam elements fixed onto the two parts in order to replicate the contact between the bolt head and threaded body, see Figure 24. The contact between of the supporting frame and the “ladder ears” has been removed to allow sliding. This constitutes a conservative modeling choice as the friction between the two surfaces is neglected.

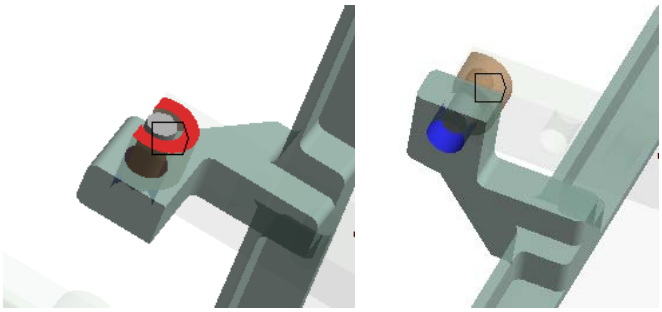

Figure 24: Bolt modeling

5.1.1.4 Boundary conditions

The CubeSat is placed in the P-POD during launch. A clearance of 0.5 mm is allowed between the P-Pod rails and the CubeSat rail. In order to model the boundary condition, a preliminary random vibration analysis is done on a model where only rail end surface is constrained, marked in red in Figure 26. The maximum deflection values after random vibration loading shown in Table 12 exceed the clearance value between the CubeSat and the P-POD. Therefore, the rails of the CubeSat are constrained in the direction normal to the rail surface as shown in Figure 25 and Figure 26.

Table 12: Maximum 3σ deflection values after random vibration - one fixed point model

Global coordinate	Maximum deflection [mm]
X direction	6.3
Y direction	4.8
Z direction	1.6

Table 13: Constraints applied on model, see Figure 25 andFigure 26.

Color	u_x	u_y	u_z
	0	0	0
	Free	Free	0
	Free	Free	Free
	0	Free	Free
	Free	0	Free

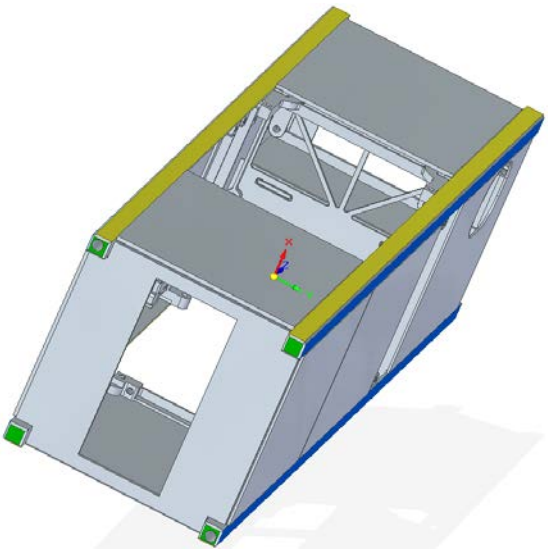

Figure 25: View from the bottom of boundary conditions

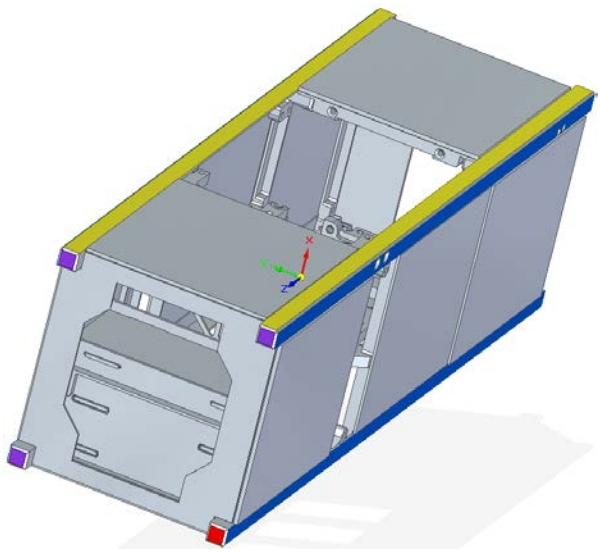

Figure 26: View from the top of boundary conditions

5.1.1.5 Loading

5.1.1.5.1 Load case one

The structure is loaded with a quasi-static load corresponding to the maximum longitudinal and lateral acceleration, see Table 14. The orientation chosen is the one creating the maximum stress values.

Table 14: Quasi-static loading

Global coordinate	Acceleration [G]
X direction	+5
Y direction	+10
Z direction	+5

The structure is simultaneously excited in the three directions using the NASA Qualification random vibration level spectrum with a constant damping factor ζ of 5% as per NASA standard [4].

Table 15: NASA Acceleration spectrum density for qualification level, payload under 22.7 kg [1]

Frequency [Hz]	ASD Level [g^2/Hz]
20	0.026
50	0.16
800	0.16
2000	0.026

5.1.1.5.2 Load case two

The structure is excited in the three directions using the Spaceflight shock response spectrum; see Table 6, with a constant damping factor ζ of 5% as per NASA standard [4].

Table 16: Shock spectrum for 1st payload shock separation transmitted to the P-POD side plate [6].

Frequency [Hz]	Acceleration [g]
100	24
270	195
2000	775
10000	775

5.1.2 Results

5.1.2.1 Modal analysis

The modal analysis is performed to determine the most predominant modes by examining the participation factor for each natural frequency, see Figure 27. The participation factor is an indication of the modal mass.

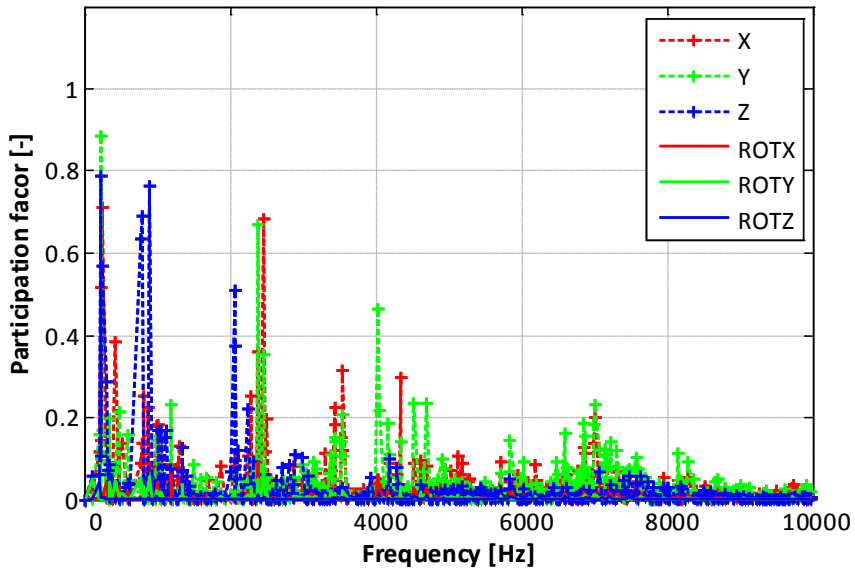

Figure 27: Participation factor as a function of the natural frequency for the CubeSat structure.

The first two mode shapes are presented in Figure 28 and Figure 29. As shown in these figures, the boom supporting frame and the "ladder ears" are prone to deformation given the importance of the two mode shapes.

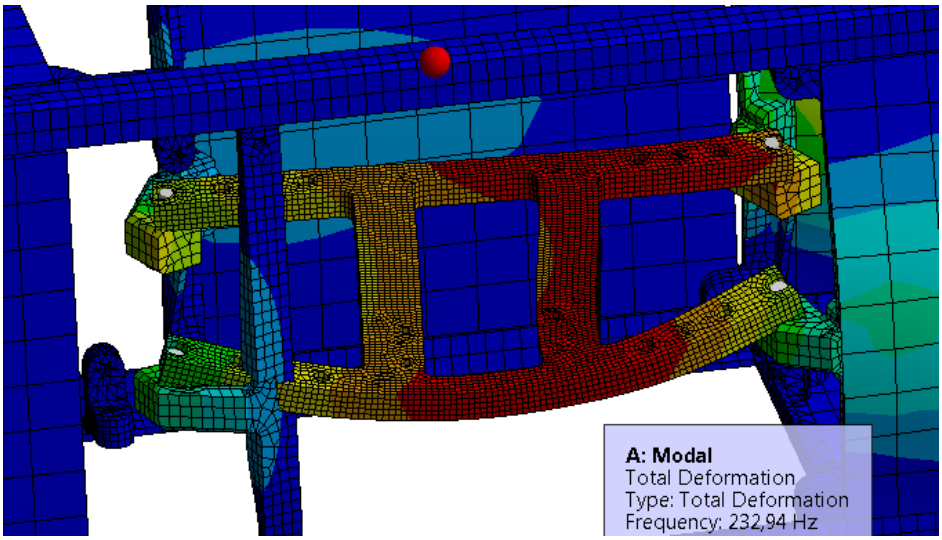

Figure 28: First predominant mode for the CubeSat structure – Mode 4 – 232.94 Hz

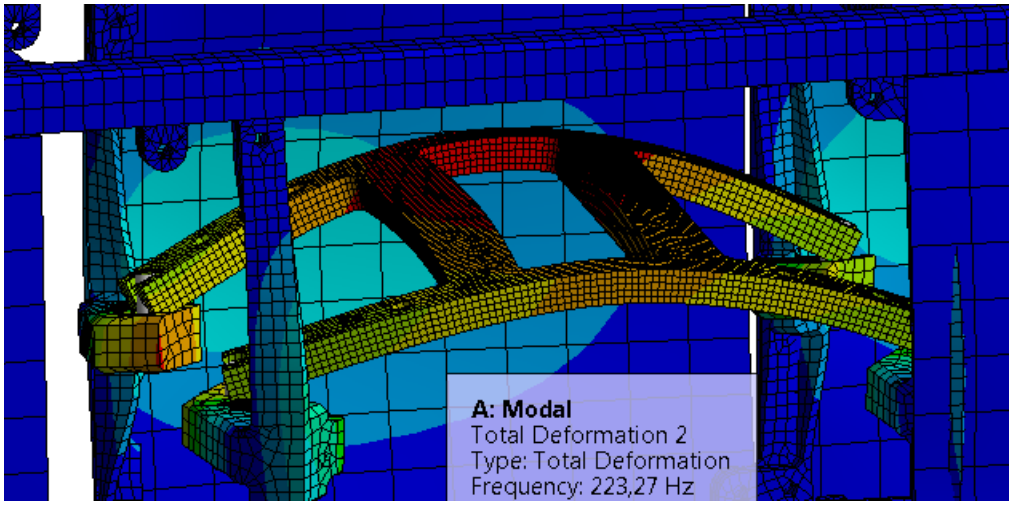

Figure 29: Second predominant mode for the CubeSat structure – Mode 3 – 223.27 Hz

5.1.2.2 Stress levels and safety factor

The 3σ analysis for the random vibration is presented in Figure 30 for the aluminum parts. The ladder parts attached to the supporting frame consist a sensitive area where stress values are highest, see Figure 30.

As the stress distribution is comparable for the static and shock loads, the shock and static stress levels are shown for these parts in Appendix 1.

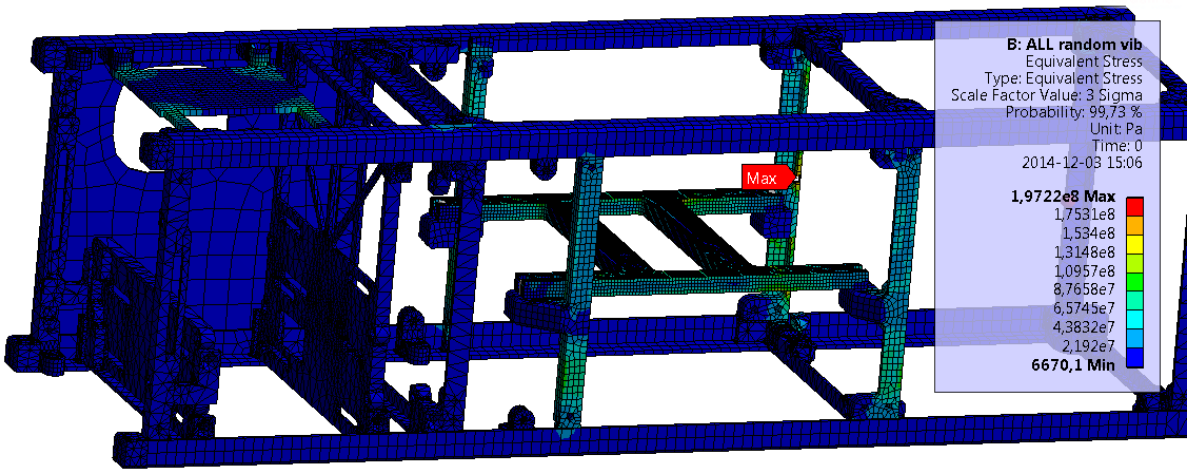

Figure 30: RMS Von Mises 3σ stress level after random vibration loading for the aluminum parts

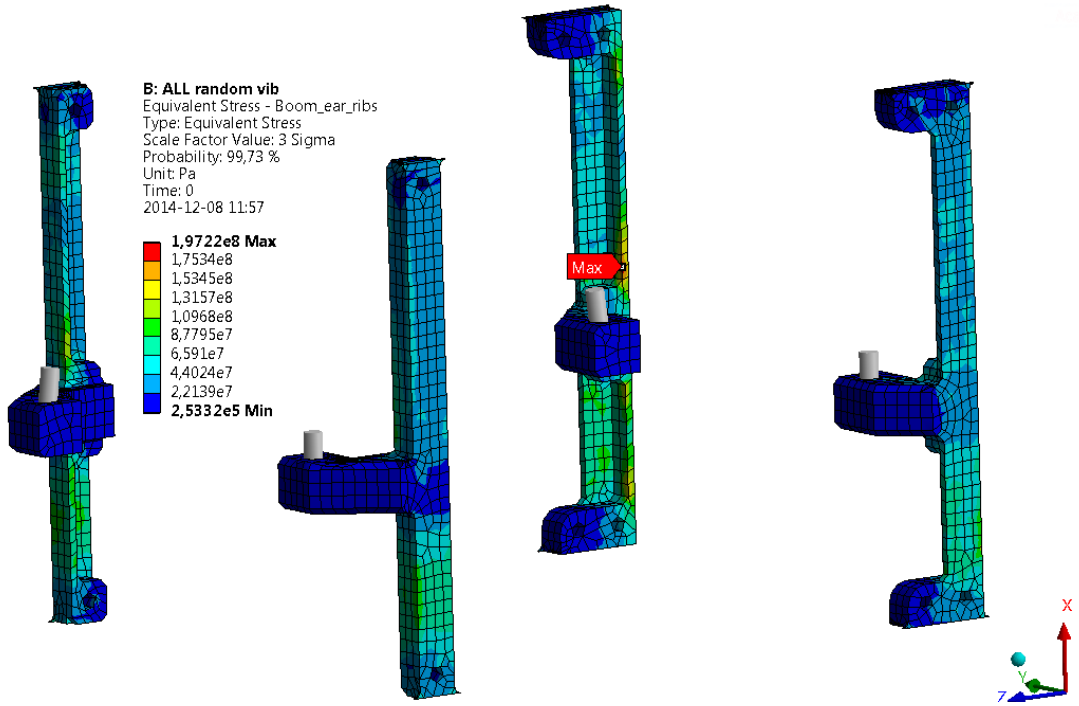

Figure 31: RMS Von Mises 3σ stress level after random vibration loading for “ladder" parts supporting the boom.

The stress values are combined for each point and the maximum value and its position in the global coordinate system are extracted and used to calculate the safety factor, see Table 17.

Table 17: Maximum stress value and safety factors for load 1 and 2

Load case	**Material**	**Maximum VM stress value for a 3σ RV analysis [MPa]**	**Maximum stress node global coordinate [mm]**			**Material Yield strength [MPa]**	**Safety factor Eq.(62)**	**X Eq.(64)**
			X	**Y**	**Z**			
Load case 1	AL7075-T6	230.5	1.61	44.20	-69.80	510	2.2	7.2
Load case 2	AL7075-T6	359.5	1.61	44.20	-69.80	510	1.4	-

5.1.3 Discussion

The results in Table 17 indicate that the CubeSat structure will withstand the first loading condition, which is to say the static requirement and the random vibration requirements for a 3σ analysis. This result reflects a conservative approach. The values chosen for the applied loads are very high as mentioned in 4.3, the masses used for the point masses reflects the highest values in the mass budget for this project. Finally, the safety factors are calculated in a very conservative manner as the von Mises stress values are just added together. Furthermore, only the maximum stress value of the whole structure is retained to calculate the safety factor.

The safety factor obtained for the shock analysis is under the minimum required value of 1.56. However, the value of the shock response spectrum needs to be validated when the launch rocket has been confirmed and precise information is available on the impact of the first separation shock on the CubeSat depending on how the nanosatellite is fixed. Furthermore, shocks are very briefs events. The material model here is linear and does not take into account viscoelastic material properties that could be of significance in the deformation mechanism.

The structure's damping factor used during the simulations is assumed. This value can only be determined by testing the structure. This value should be determined in order to confirm the simulation results.

As shown in Figure 29, some penetration issues are observed, due to the linear nature of contacts in these simulations. In fact only bounded/no slip contacts or the absence of contact is allowed for this type of analysis which leads to an over-constrained model on one hand or an under-constrained model on another hand. The fact that the contact between the support frame and the ladder ensure a conservative approach since the possible physical displacement is overestimated.On the other hand, the bounded contact between the ladder and the solar panels added extra stiffness. Contacts with friction would have been more representative. However, this contact is not allowed during modal analysis due to its non-linearity. The same reflection is applicable to the screw fixations. Apart from the supporting frame / ladder connection, all the screw assemblies have been substituted by bounded contacts which can over-constrain the model. Furthermore, screw fixation need to be tested as screws can loosen up during vibrations tests.

The point masses are linked with rigid links to the structure which could over-constrain the model. In order to determine if this assumption is correct, each block represented by a point mass should be tested individually and compared to its corresponding simulated behavior.

The simulations have allowed to detect sensitive areas and to adjust the design of the aluminum structure accordingly.

5.2 Star tracker

The star tracker is an instrument enabling to navigate the CubeSat by taking pictures of the star constellations, then used to determine the position of the satellite. A conservative local analysis is conducted on this instrument consisting of aluminum, FR4CW circuit board and an optical block consisting of lenses. Only stress values in the aluminum parts are of interest in this project and therefore are presented here.

5.2.1 Model

The complex star tracker structure is modeled in order to simulate the two load cases. This analysis is linear.

5.2.1.1 Geometry and material

The different part names and their linear elastic material parameters are presented in Table 18 and Figure 32. The local coordinate system is shown in Figure 32.

Table 18: Star Tracker material properties

Item	Item color in figures	Material	Elastic Modulus [GPa]	Poisson's ratio	Tensile strength [MPa]	Ultimate strength [MPa]	Density [kg/m^3]
Star tracker plate	Blue	AL6082-T6	70	0.33	230	310	2700
Vanes	Red	AL6082-T6	70	0.33	230	310	2700
C-mount	Yellow	AL6082-T6	70	0.33	230	310	2700
Lens block	Cyan	Lens block	64	0.2	-	-	2400
Electronic board	Orange	FR4CW	23.4	0.14	-	-	4200

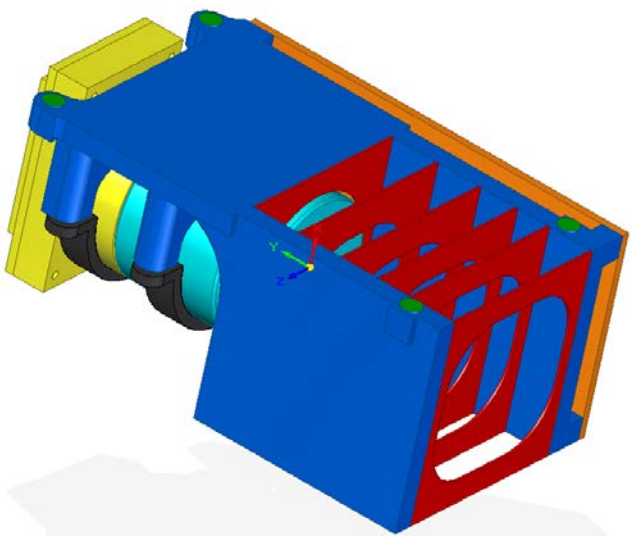

Figure 32: Star Tracker

5.2.1.2 Meshing and contact

The structure is meshed in order to reduce the number of nodes in non-sensitive areas and increase the mesh quality in the region of interest and sensitive contact areas, see Figure 33 and Figure 34.

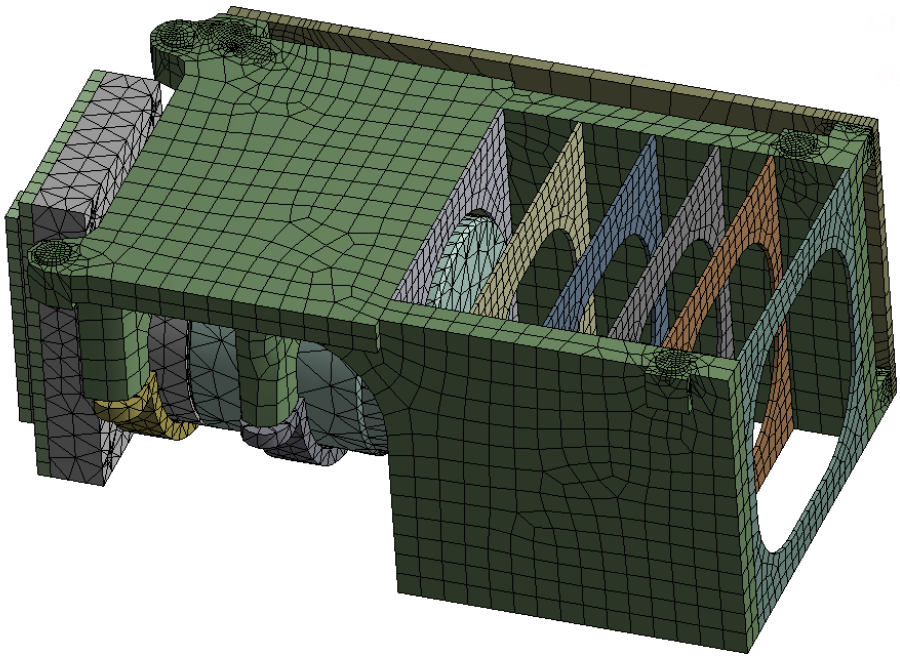

Figure 33: Star Tracker mesh - view A

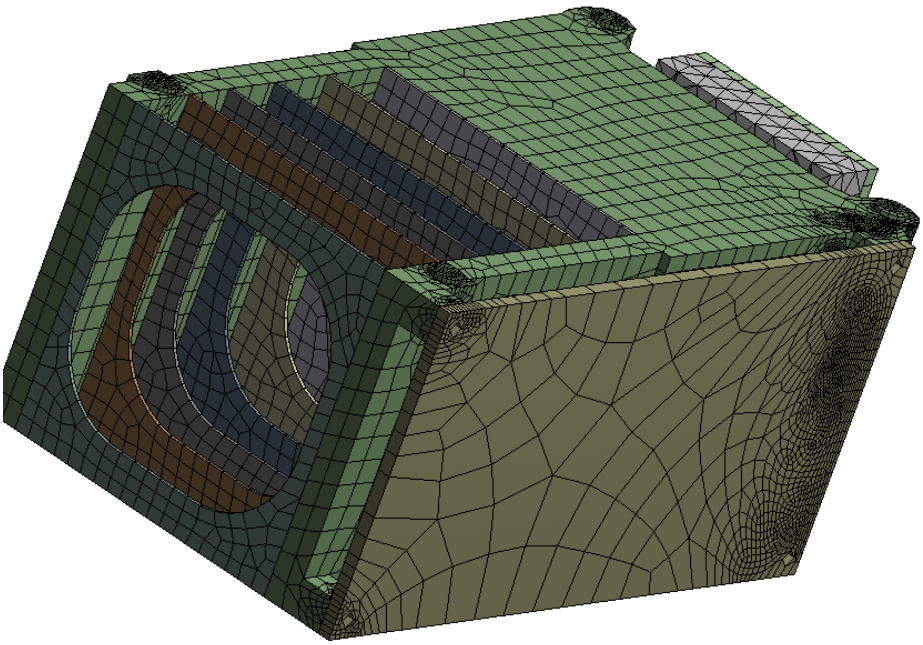

Figure 34: Star Tracker mesh - view B

The structure has been meshed with different element types listed in.

Table 19: Meshing parameters

Element name	Shape	Number of nodes per element	Degree of freedom per node	Structural components meshed with element type
SOLSH190	Hexahedral	4	3	Vanes, Electronic board
SOLID185	Hexahedral	8	3	Star tracker plate, electronic
SOLID187	Pyramidal	10	3	Lens block, C-mount
BEAM188		2	6	Screws
TARGE170		N/A	N/A	All bounded contacts
CONTA174		N/A	N/A	

The analysis is linear and therefore all contacts are no slip/ bounded contacts.

These screws have been modelled as beam elements fixed onto the two parts see Figure 35.

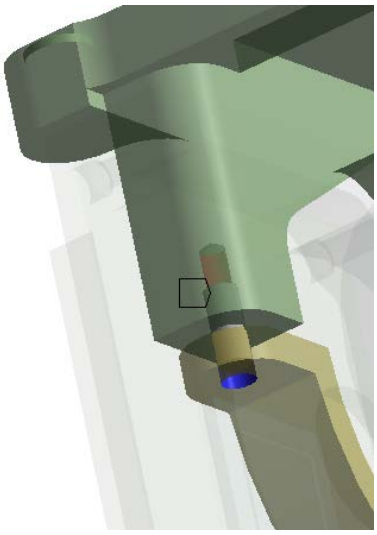

Figure 35: Screw modeling, placement indicate by the back arrow.

5.2.1.3 Boundary conditions

Four circular areas representing the placement of screws are fixed which is to say that all 6 DOF are constrained in these areas, see green dots in Figure 32.

5.2.1.4 Loading

The loading conditions are identical to the ones applied and the CubeSat structure and can be found in 5.1.1.5.

5.2.2 Results

The von Mises stress results are shown for the 3σ analysis for the random vibration in Figure 36, for the static loading in Figure 37 and for the shock analysis in Figure 38.

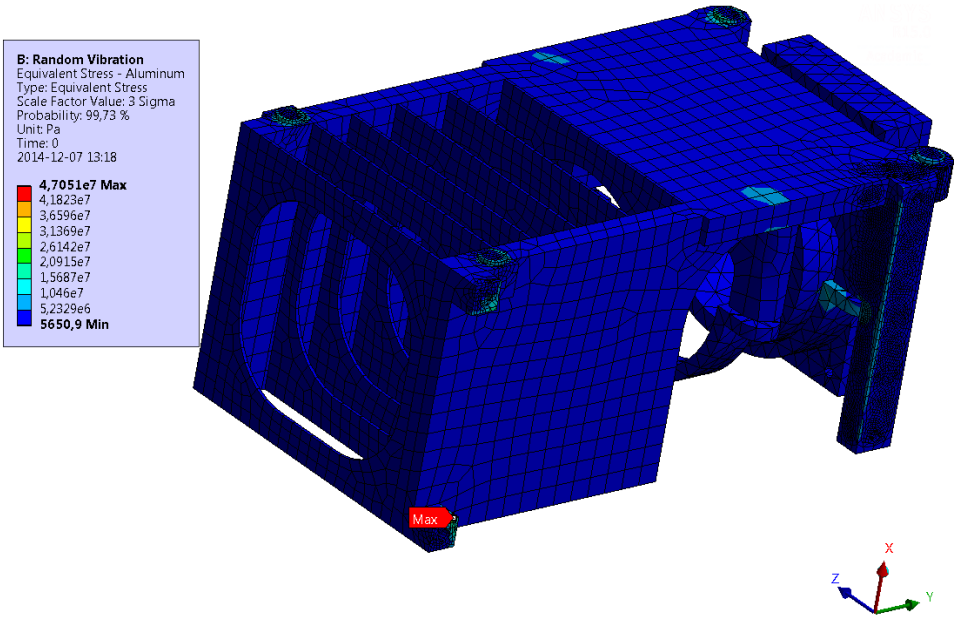

Figure 36: RMS Von Mises 3σ stress level after random vibration loading for the aluminum parts

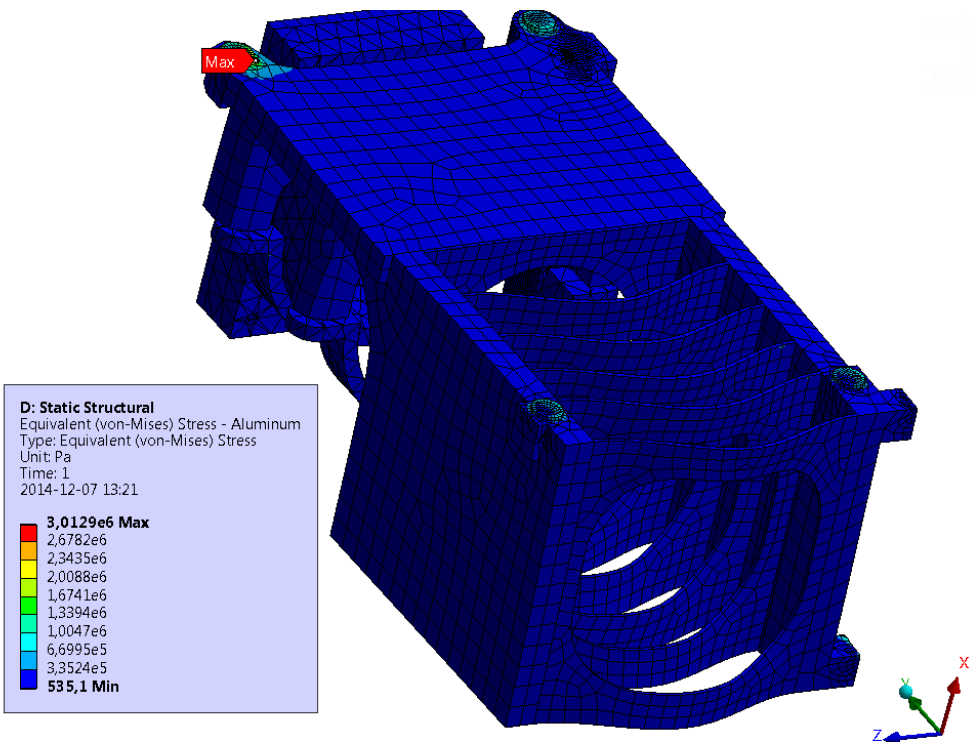

Figure 37: Von Mises stress level after static loading for the aluminum parts

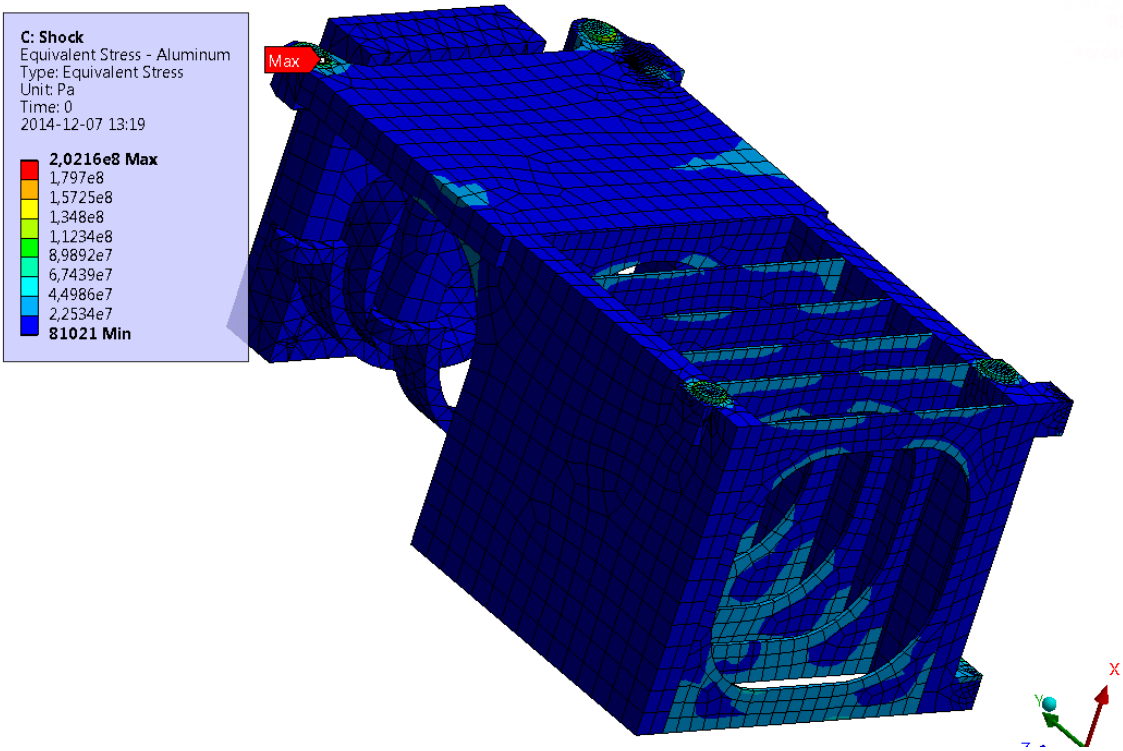

Figure 38: Von Mises stress level after shock loading for the aluminum parts

The stress values are combined for each point and the maximum value and its position in the global coordinate system are extracted and used to calculate the safety factor, see Table 17.

Table 20: Maximum stress value and safety factors for load cases 1 and 2

Load case	Material	Maximum VM stress value	Maximum stress node local coordinate [mm]			Material Yield strength	Safety factor	x
		[MPa]	X	Y	Z	[MPa]		
Load case 1	AL6082-T6	48.3	-24.16	-32.06	-36.40	230	4.8	14.5
Load case 2	AL6082-T6	202.1	11.94	46.10	12.00	230	1.1	-

5.2.3 Discussion

The results presented in Table 20 indicate that the final design will withstand the first loading condition, which is to say the static requirement and the random vibration requirements for a 3σ analysis. The vibrations are applied directly on the four points representing screw fixations. This simplification does not take into account the damping of the acceleration level by the CubeSat structure before it is transmitted to the Star Tracker and in this sense makes the approach conservative.

The safety factor obtained for the shock analysis is under the minimum required value of 1.56. However, the value of the shock response spectrum needs to be validated when the launch rocket has been confirmed and precise information is available on the impact of the first separation shock on the CubeSat depending on how the nanosatellite is fixed. Furthermore, shocks are very briefs events. The material model here is linear and does not take into account viscoelastic material properties that could be of significance in the deformation mechanism.

The stress concentration point found in Figure 36 is due to contact conditions between the PCB plate and the aluminum frame and should not be of such high value in reality.

The lens block is modelled according to its mass and stiffness but the lenses are not modelled. These items should be tested as glass as material and include micro cracks that could propagate due to random vibration loading.

Considerations presented in 5.1.3 regarding loading, safety factor calculation, damping factor, meshing and contact considerations are also valid for this model.

5.3 Boom plate assembly

The thin FR4 front plate of the boom plate is in its design process. The thickness of this plate is of interest. The plate should not touch the back thick FR4 plate during random vibration loading. Therefore an analysis is conducted for different values of thickness.

5.3.1 Model

There are two boom plate assemblies symmetrically situated on top of the deployable boom structure, see Figure 39.

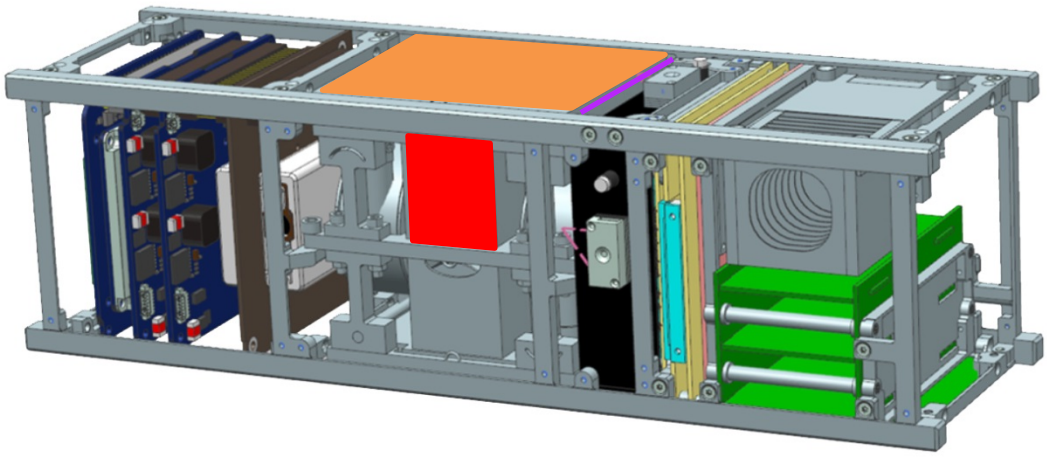

Figure 39: Boom thin plate position (orange), boom thick plate (purple) and block (purple) positions in the CubeSat

5.3.1.1 Geometry and model parameters

The boom plate assembly consists of a thin and a thick FR4 plates as well as a block. The plates are separated with a 0.5 mm gap. This gap is created by small rings 0.5 mm thick. The two plates are attached together by screws and nuts represented by cylindrical slices, see component description in Table 21, Figure 40 and Figure 41. Both the screws assembling the plates together and the screws mounted on the block are modelled as cylindrical slides of 0.5 mm thickness, see Figure 41. The material model is linear elastic.

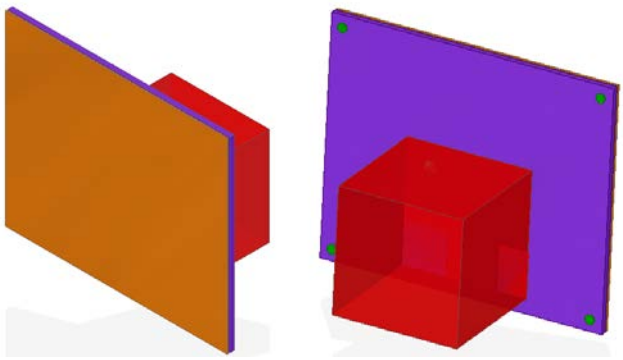

Figure 40: Boom plate mechanism front and back

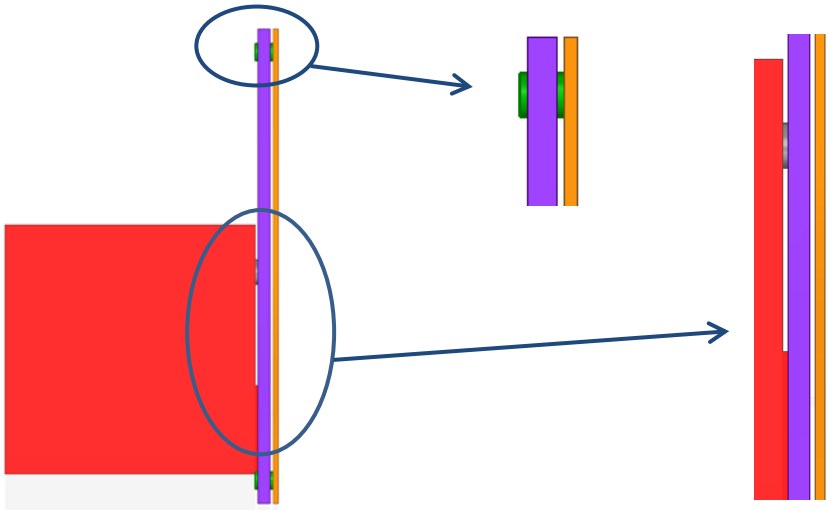

Figure 41: Separators between the thin and the thick plate. Glue and screw between the sensor block and the thick plate

Table 21: Structural component material properties

Item	Material	Item color	Dimension L x W x H [mm]	Elastic Modulus [GPa]	Poisson's ratio	Yield strength [MPa]	Density [kg/m^3]
Thin plate	FR4	Orange	95 x 80 x0.5,0.9	24,3	0,14	65	1850
Thick plate	FR4	Purple	95 x 80 x 2	24,3	0,14	65	1850
Block	Block material	Red	42 x 42 x 42	24,3	0,14	65	1027
Separators	Aluminum	Green	Ø 3 x 0.5	70	0,33	276	2700
Screw	Aluminum	Green	Ø 4 x 0.5	97	0,31		8490

5.3.1.2 Meshing and contact

The areas of interest are the thin plate and the contact between the sensor block and the thick plate. Therefore the mesh in these areas have been refined, see Figure 42 and Figure 43. The analysis is linear and therefore all contacts are no slip/ bounded contacts.

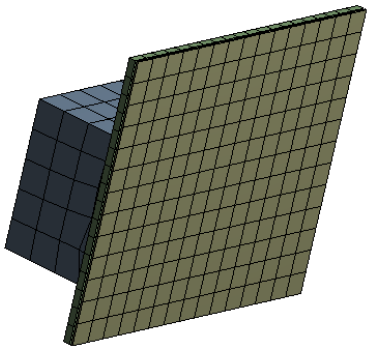

Figure 42: Thin plate meshing

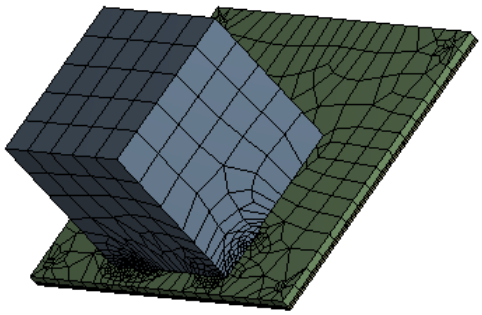

Figure 43: Block meshing and refined meshing around contact area

5.3.1.3 Boundary conditions

Four circular areas representing the placement of screws are fixed which is to say that all 6 degrees of freedom are constrained in these areas, see green dots in Figure 44.

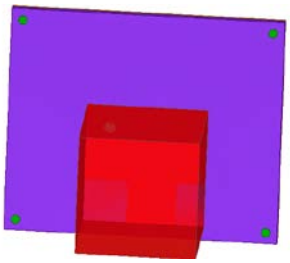

Figure 44: Fixed areas in green where all DOF are constrained.

5.3.1.4 Loading and damping factor

The structure is excited in the three directions using the NASA Qualification level spectrum with a constant damping factor ζ of 5% as per NASA standard [4].

5.3.2 Results

The out of plane displacement for the thin plate is of interest and presented for two cases in Figure 45 and Figure 46 for different thicknesses. The results show that only the thin plate show an out-of plane deflection for the random vibration loading and therefore is presented here in Table 22.

Table 22: Maximum out-of-plane deflection for the thin plate

Thin plate thickness [mm]	Max out-of-plane displacement [mm]
0.5	0.70
0.7	0.43
0.9	0.30

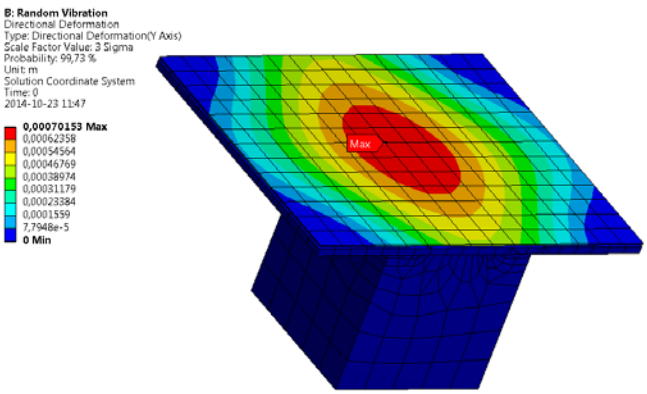

Figure 45: Out of plane deformation for the top thin plate – Plate thickness 0.5 mm

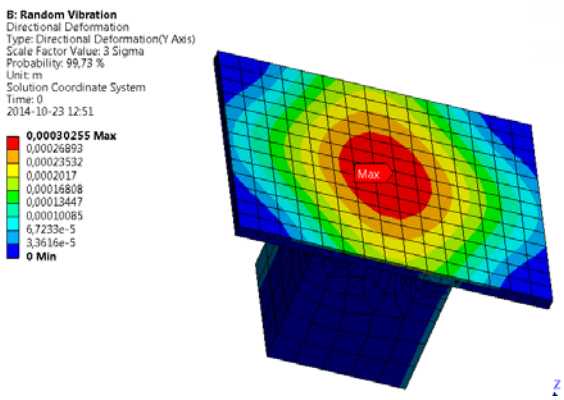

Figure 46: Out of plane deformation for the top thin plate – Plate thickness 0.9 mm

The aim of the design is to prevent the thin plate to touch the thick underneath plate and therefore a 0.9 mm plate is chosen as final design.

5.3.3 Discussion

Table 22 indicates that the thin plate will be not touch the thick plate due to the random vibration loading condition for a plate thickness of 0.9 mm with an adequate safety factor. However, the static load due to the acceleration of the rocket and when applied in compression normal to the thin plate surface could increase the deflection. The additional loading could be of consideration for another study.

Random vibration loading condition is applied directly on the four points representing screw fixations. This simplification does not take into account the damping of the acceleration by the CubeSat structure before it is transmitted to the boom assemblies and in this sense makes the approach conservative.

Considerations presented in 5.1.3 regarding loading and damping factor considerations are also valid for this model.

6 Conclusions

6.1 Identify test levels

The most challenging aspect of space design is to identify loads. With prohibitive launch costs, real life test data is not available for a project such as the SEAM CubeSat project. Different information sources are available in form of standards by NASA [4], other space agencies and launch provider documentation [1]. As CubeSats are secondary payloads, little information is available concerning the loading conditions specifically applicable to this kind of satellite. Only in recent years specifications have been published for CubeSat and secondary payload in general [5][6].

In order to use these standards, the launch process needs first to be analyzed to understand which loads are applicable to the structure of interest, at what level and if some loading conditions occur simultaneously. The SEAM Cubesat project is in a design phase where the actual launch rocket and position of the satellite in the rocket are still unknown. Therefore, simulations have been carried out from load spectrum levels considered applicable to this kind of satellite with a “worst case scenario approach”, see 4.3.6.

6.2 Method

The CubeSat structure, Star Tracker and boom plate have been modelled. Thereafter static, random vibration and shock response spectrum analysis have been conducted on these structures in Ansys Mechanical in Ansys Workbench 15.0.

In order to simulate the different load cases, the geometry has been simplified using point masses which values were calculated in a conservative manner for the CubeSat using CAD model and the mass budget of the satellite for the corresponding replaced components. As the point masses have been attached with rigid beams to the structure, the accuracy of the stiffness of the group of replaced components needs to be compared to physical test values to confirm the assumption.

As linear analyses are conducted, the only contacts option is bounded/no slip contacts or the absence of contact. Screw contact is not modelled only for a few cases in sensitive areas, see 5.1.1.3. and 5.2.1.2. For example in the case of the solar panels, the bounded contact attaching them to the structure will slightly over constrain the model compared to reality.

Boundary conditions are also determined due to physical properties like contact between the CubeSat dispenser of P-POD rails and the structure but also out of linear contact considerations which added stiffness to the model compared to reality.

The model is then meshed in order to focus on the areas of interest and given computing restrictions for the software used.

Stress or displacement values are extracted for the different models; the initial designs have been modified in the case of the CubeSat structure and the boom plate to prevent stress concentration or to unwanted contact respectively, see 5.3.2.

6.3 Safety factors

The minimum safety factor is determined by using NASA standard and identifying the factors applying in this project. The minimum safety factor is determined to be 1.56.

The load cases are determined in 4.3.6. Safety factors against initiation of plastic deformation are calculating in a deterministic way by linearly adding static and dynamic load for load case 1 and using the stress value coming from the shock analysis in load case 2. A statistic approach is also considered for load case 1 where static von Mises stress is combined with the RMS von Mises stress from the random vibration analysis. In this case, the number of standard deviations x required for the material to initiate plastic deformation is also calculated and presented in the table below as a summary of Table 17 and Table 20.

Structure	Load case	Material	Maximum VM stress value for a 3σ RV analysis [MPa]	Material Yield strength [MPa]	Safety factor Eq.(62)	X Eq.(64)
CubeSat structure	Load case 1	AL7075-T6	230.5	510	2.2	7.2
	Load case 2	AL7075-T6	359.5	510	1.4	-
Star tracker	Load case 1	AL6082-T6	48.3	230	4.8	14.5
	Load case 2	AL6082-T6	202.1	230	1.1	-

The minimum safety factor requirement is not met for load case 2 (shock simulation). However, the material model used is linear. The brief duration may introduce time dependent phenomenon like viscoelasticity may be reducing the deformation and the stress physically observed in the material after this kind of loading.

7 Final words

The CubeSat structure was designed to sustain the launch load conditions, random vibration and steady state loading. Shock spectrum simulations have shown that the structure could be subjected to plastic deformation. These simulations have been providing good insight of some of the mechanically sensitive or weak areas.

However, this project is still at its design phase and a number of parameters still need to be confirmed. The damping values and the loading conditions are still assumptions. The shock spectrum values represent the best information available at the time of this Master thesis but need to be confirmed. This simulated model is to be compared with physical test to confirm modeling assumptions.

This work could help further CubeSat projects in identifying the mechanical requirements on this structure, which ones apply to this kind of structure and how to combine static and dynamic loads.

References

[1] Arianespace (2006), *SOYUZ from the Guiana space center user's manual*.

[2] J. Michaud et al (June 2013), *Piggybacking Arianespace launches: a cost efficient opportunity for planetary smallsats*, ThalesAlenia Space, LCPM-10 – Pasadena – June 18th-20th, 2013 - http://www.lcpm10.caltech.edu/pdf/session-6/4_session%206_billot_oral_V2%20+ComJM.pdf, 2014-10-15

[3] http://www.ltasvis.ulg.ac.be/cmsms/uploads/File/CALVI_Students_LIEGE_2011_6%281%29.pdf, 2014-09-16

[4] NASA (2005), *General environmental verification standard (GEVS) For GSFC Flight Programs and Projects*, NASA GSFC-STD-7000.

[5] NASA (Jan 2014), *Launch Services Program – Program Level Dispenser and CubeSat Requirements Document*, LSP-REQ-317.01 Revision B

[6] Spaceflight, Inc. (2013), *Secondary Payload Users Guide*, SF-2100-PUG-00001, Rev D 2013-03-05.

[7] J. Wijker (2009), *Random Vibrations in Spacecraft Structure Design, theory and applications,* ed. Springer.

[8] T.Irvine (2007), Methods for converting a power spectral density to a shock response spectrum, http://www.vibrationdata.com/tutorials/psd_srs.pdf, 2014-11-20

[9] A. C. Nilsson (2000), *Vibroacoustics*, Department of Vehicle Engineering, KTH, Stockholm, Sweden.

[10] W. Weaver Jr (1990) *Vibration problems in engineering, fifth* edition.

[11] S. Khoshparvar (2010), *Random vibration stress analysis of the BepiColombo wire boom deployment system*, Master thesis, Stockholm, Sweden.

[12] D.J. Segalman et al. (2000), *An efficient method for calculating rms von Mises stress in a random vibration environment*, Journal of Sound and Vibration 230(2), 393-410.

[13] SAS IP (2014), *ANSYS Manual - Mechanical APDL/Theory reference/15.7.11.4. Equivalent Stress Me*an Square Response.

[14] M. Pearce (2014) *Enclosure 3: SNSB call 2013-IS: 'SPHiNX: Segmented Polarimeter for High eNergy X-rays', Instrument specification and development*, Februrary 2014.

[15] http://fp7-seam.eu/, 2014-10-15

[16] NPO Lavochkin (2014), *Loading environment for small SC (secondary payloads)*, Lavochkin Research and Production Association, Chimki

[17] S. Rubin (2002), *Concepts in Shock Data Analysis*, McGraw-Hill, New York.

[18] D. Steinberg (1988), *Vibration Analysis for Electronic Equipment*, John Wiley & Sons.

[19] http://www.edr.no/blogg/ansys_bloggen/ansys_tutorial_earthquake_analyses_in_workbench. 2014-09-01

[20] SAS IP (2014), *ANSYS Manual - Mechanical APDL/Theory reference/15.7.3. Single-Point Response Spectrum.*

[21] ECSS (2009), Space engineering - *Structural factors of safety for spaceflight hardware*, ECSS-E-ST-32-10C Rev.1.

[22] N. Bouras et al (1999), *Thermal shock properties of chemically toughened borosilicate Glass*, Journal of Non-Crystalline Solids 247 p 39-49.

[23] J. Faleskog, specialized in Fracture Mechanics, KTH, Department of Solid Mechanics, Sweden, *Private communications*, 2014-09-25.

[24] B. Sundström, ed. (2010) *Handbook of Solid Mechanics*, Department of Solid Mechanics, KTH, Stockholm, Sweden. pp. 269.

[25] R. Simmons (2001), *Miles' Equation*, NASA Goddard Space Flight Center.

[26] H. SHEN el al (2012), *Growth, Mechanical and Thermal Properties of Bi4Si3O12 Single Crystals*, School of Materials Science and Engineering, Shanghai Institute of Technology, Shanghai 201418 CHIN. PHYS. LETT. Vol. 29, No. 7 (2012) 076501.

[27] http://www.hamamatsu.com/jp/en/search/index.html?spkey=R7600U&searchBtn.x=0&searchBtn.y=0 , 2014-10-13

[28] http://www.nasa.gov/directorates/heo/home/CubeSats_initiative.html#.VLOwFnv3SDk, 2014-10-15

Appendix 1 CubeSat simulations additional results

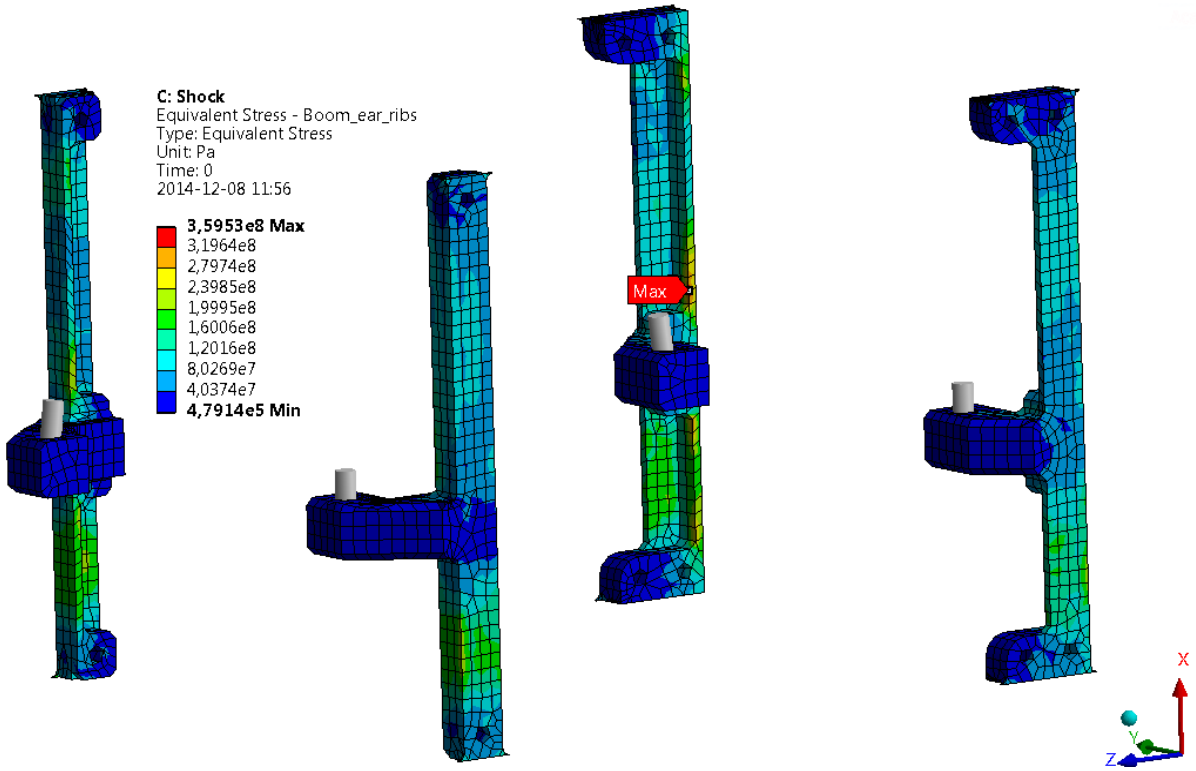

Figure 47: Von Mises stress after shock response spectrum loading for the ladder parts supporting the frame.

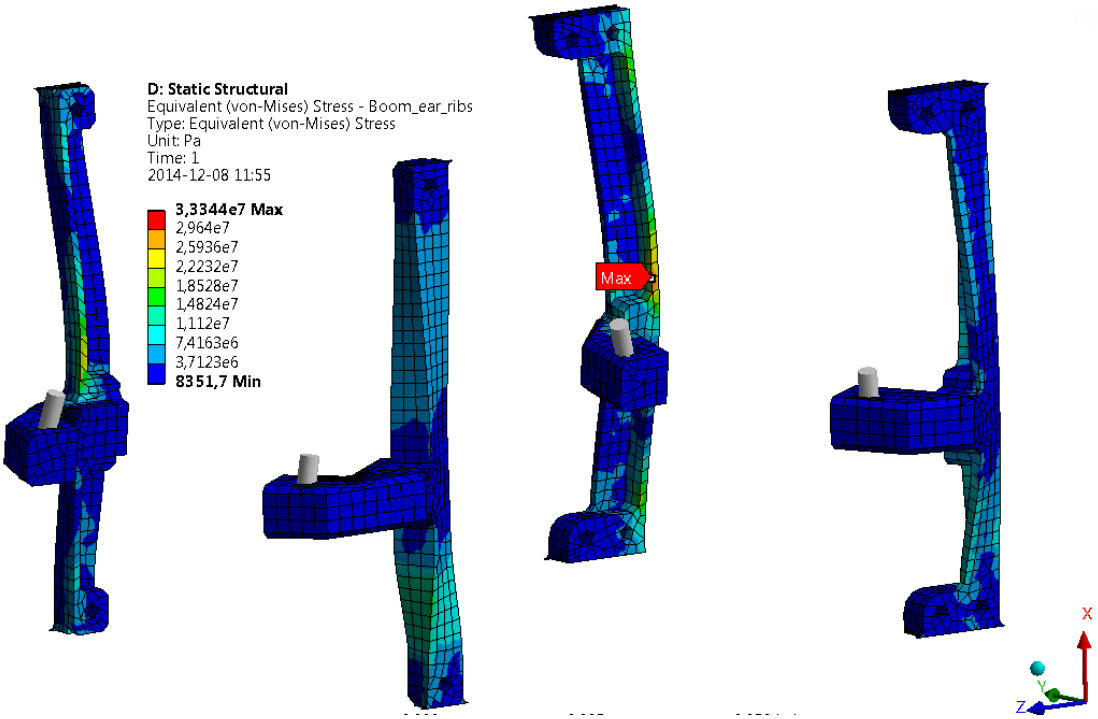

Figure 48: Von Mises stress after static loading for the ladder parts supporting the frame.

Appendix 2 Comparison between random vibration stress analysis and Mile's equivalent acceleration induced stress.

Plate example

A steel plate with parameter listed in Table 23 is studied in order to compare RMS von Mises stress values from a random vibration analysis in Ansys and the stress generated from GRMS acceleration applied on the structure from the Mile's equation.

Table 23: Plate model parameter

Dimension L x W x H [mm]	100 x 10 x 1
Elastic Modulus [GPa]	200
Poisson's ratio	0.3
Density [kg/m^3]	7850

The structure is meshed with 1mm^3 SOLID186 elements. This element is defined by 20 nodes having three degrees of freedom per node. The modal frequencies are extracted from Ansys. The found frequencies are 82, 514, 810, 1440, 1550, 2823, 4668, 4675, 4861, 6976 Hz. The predominant modes are the 1st mode for the out-of plane deflection and the 3rd mode for the in-plane deflection.

The plate is then loaded with the random vibration spectrum seen in Figure 49.

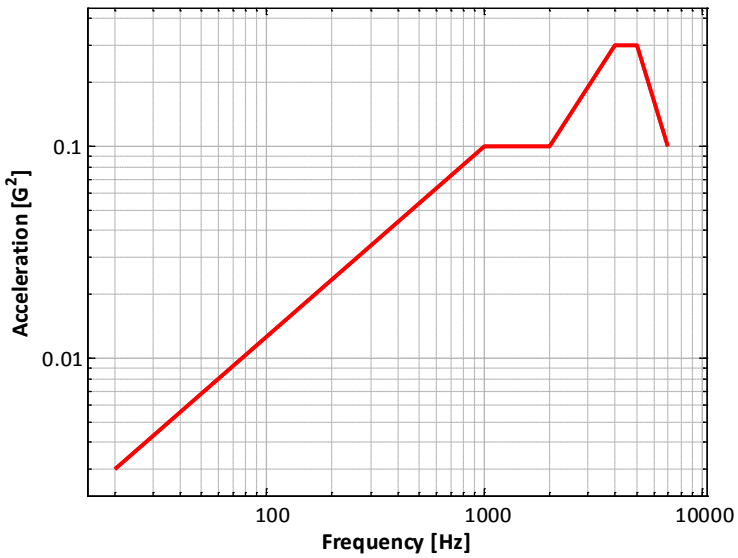

Figure 49: Spectrum used for the plate

Out of plane results

The maximum RMS von Mises (VM) stress is extracted for a given number of modes and compared to the von Mises stress equivalent generated from the Mile's equation equivalent GRMS acceleration shown see Figure 50.

Figure 50 shows that the Mile's equation is overestimating the von Mises stress when the modes other than the first mode used to calculate the GRMS values. This is consequent with the 1st mode being predominant for this direction. Figure 51 and Figure 52 show that in the stress distribution is comparable for the random vibration and the Mile's equivalent acceleration clearly indicating how the first bending mode is the main contributor in this case.

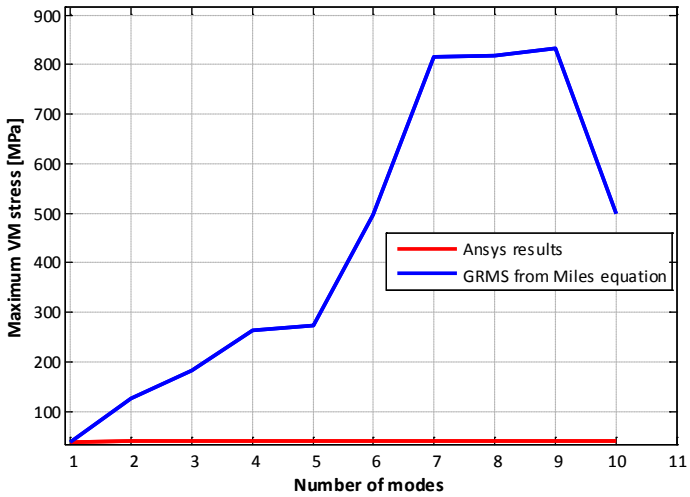

Figure 50: Maximum 3σ RMS von Mises Stress: simulation in Ansys and static equivalent GRMS from Mile's equation – Out of plane

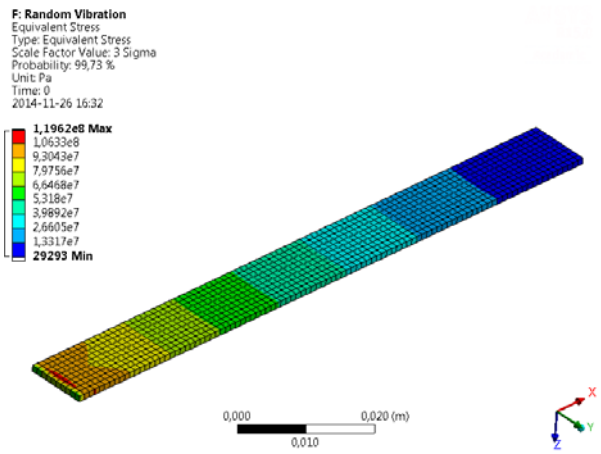

Figure 51: 3σ RMS von Mises stress for 10 modes - out-of-plane excitation

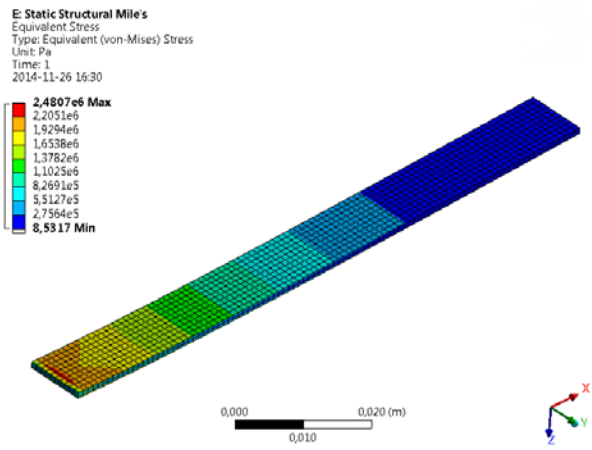

Figure 52: Von Mises stress – 1G out-of-plane acceleration

In- plane results

In the same manner, the VM stresses for the two analyses are compared as shown in Figure 53. Figure 53 shows that the Mile's equation is overestimating the von Mises stress. However, when only 3 modes are taken into account, the two stress levels are comparable. This is consequent with the 3rd mode being predominant for this direction. Figure 54 and Figure 55 show that in the stress distribution is comparable for the random vibration and the Mile's equivalent acceleration clearly indicating how the third mode is the main contributor in this case.

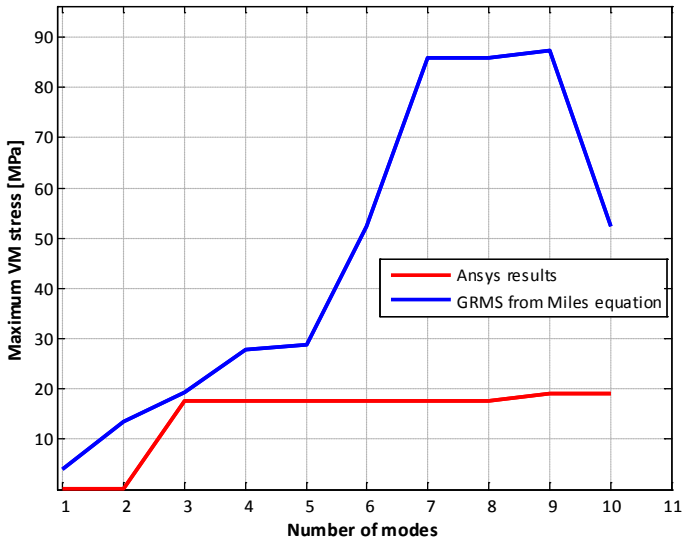

Figure 53: Maximum von Mises Stress: simulation in Ansys and static equivalent GRMS from Miles equation – In plane

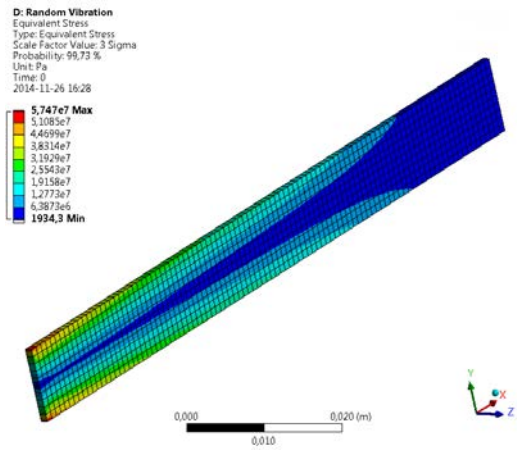

Figure 54: RMS von Mises stress for 10 modes – in-plane excitation

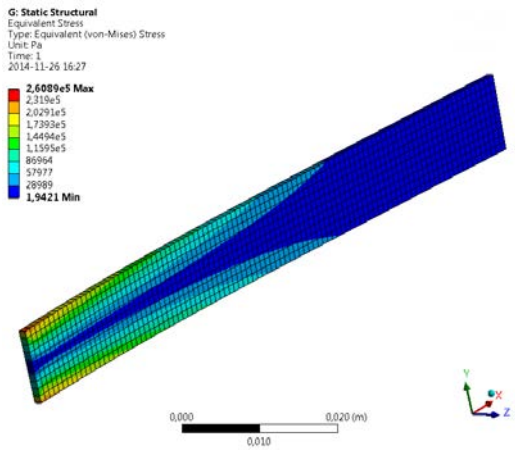

Figure 55: Von Mises stress – 1G in-plane acceleration

Pipe example

A steel pipe with parameter listed in Table 24 is studied in order to compare RMS von Mises stress values from a random vibration analysis in Ansys and the stress generated from GRMS acceleration applied on the structure from the Mile's equation.

Table 24: Pipe model parameter

Dimension L x D [mm]	100 x 10
Elastic Modulus [GPa]	200
Poisson's ratio	0.3
Density [kg/m^3]	7850

The structure is meshed with SHELL181 elements. This element is a four-noded element with six degrees of freedom at each node. The modal frequencies are extracted from Ansys and found to be 672, 672, 1630, 1630, 2151, 2151, 2590, 3130, 3130, and 3841 Hz. The modal analysis reveals that the 2nd mode is predominant.

The pipe is then loaded with the random vibration spectrum seen in Figure 56.

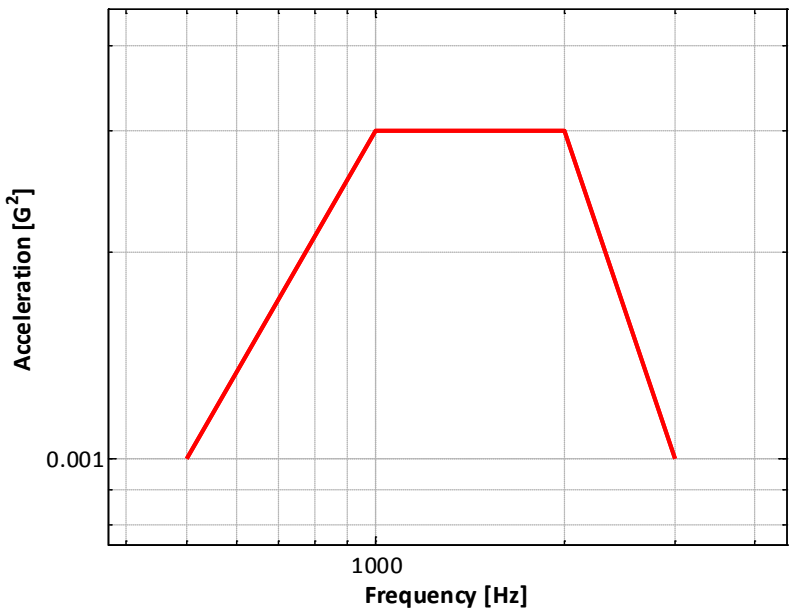

Figure 56: Spectrum used for the pipe

Figure 57 shows that the Mile's equation is overestimating the von Mises stress. However, when only two modes are taken into account, the two stress levels are comparable. This is consequent with the 2nd mode being predominant

Figure 58 and Figure 59 show that in the stress distribution is comparable for the random vibration and the Mile's equivalent acceleration clearly indicating how the second bending mode is the main contributor in this case.

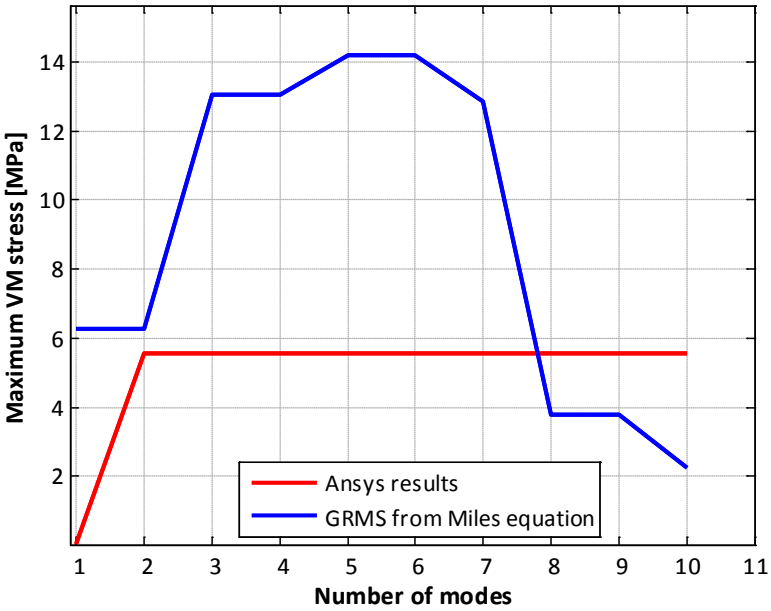

Figure 57: Maximum von Mises Stress: simulation in Ansys and static equivalent GRMS from Miles equation – z plane

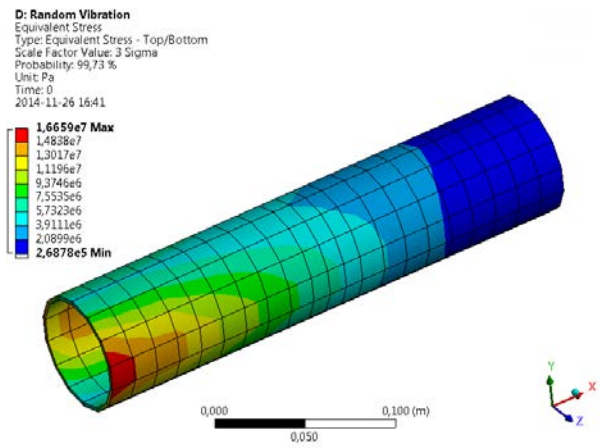

Figure 58: RMS von Mises stress for 10 modes - z-plane excitation

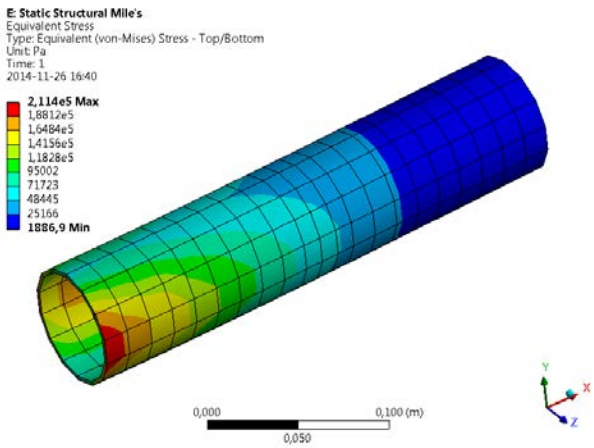

Figure 59: Von Mises stress – 1G z-plane acceleration

Appendix 3 Simulation of the SPHiNX polarimeter array

Background

SPHiNX is a Compton-based hard X-ray polarimeter for the study of gamma-ray bursts. The polarimeter is placed on a satellite, see Figure 60. The structure is subjected to mechanical loads during launch and operation. The engine generates random vibrations. The structure is also subjected to pyro shocks when the satellite is released into space. At this point, this project has not being selected for further development so the level of detail in the design is still low for this instrument.

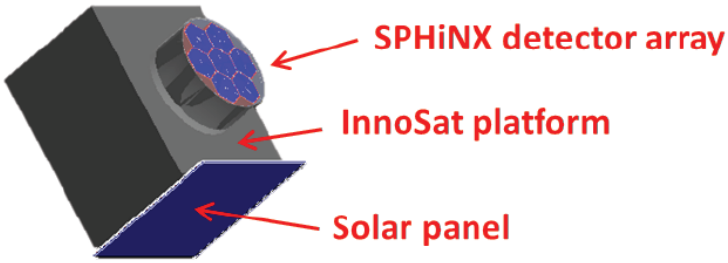

Figure 60: The simplified geometrical model with SPHINX mounted on the satellite

Model

The SPHiNX detector array with its seven honey combs structure is modelled to evaluate stresses induced by random vibrations and pyro shocks during the launch of the satellite. The analysis is linear both regarding material properties and contact assumptions.

Geometry and material parameters

The SPHiNX detector array is fitted into the satellite with a protective cover structure, see Figure 61. For the purpose of this analysis, only the detector array is modelled.

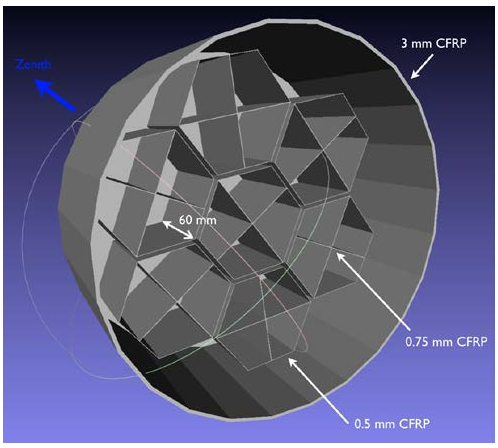

Figure 61: The SPHiNX shielding system. The outer carbon fiber shell is shown as well as the 'pockets' into which the plastic and BGO scintillators are located [14].

The SPHiNX detector array is composed of a seven unit structure covered by a lid; see Figure 62 and Figure 63. Each unit is composed of Carbon Fiber Reinforced Plastic (CFRP) walls where four plastic scintillators are placed, each attached to a photomultiplier (PMT) with a silicone pad. Material parameters are presented in Table 25.

Table 25: Material parameter for Segmented Polarimeter for High Energy X-rays

Item	**Item color in figures**	**Dimension L x W x H Thickness T [mm]**	**Elastic Modulus [GPa]**	**Poisson's ratio**	**Tensile strength [MPa]**	**Density [kg/m^3]**
PMT Hamamatsu R7600U	White	30x30x30	5 - 20 - 50	0.35	40	1040
Plastic scintillator in Plexiglas	Orange	54.4x47.3x60	3	0.35	80	1032
BGO crystals	Blue	60x27.5x4	32	0.33	N/A	7100
Lid and honeycomb structure in CFRP	Red	Lid: 288.3x300.8x1 Hexagon: 96.3x111.2x91 T:0.5 Cross:95.3x110x90.5 T:0.75	85	0.1	350	1600
Silicone pads (Silicone BGO and Silicone PMT)	Green	For BGO: 60x27.5x1 For PMT: 30x30x0.8	0,05	0.48	5	2000
Borosilicate glass	Grey	25.7x25.7x0.8	64	0.2	35	2200

The photomultiplier (PMT) is a measuring system consisting of electronic component, a borosilicate glass on its top surface and a metallic shell. A sensitivity analysis has been performed for different values of Young's modulus value of this component modelled as a homogenous block.

The borosilicate glass present in the PMT can be a sensitive component and therefore has been modelled as a separate piece fitted into the PMT unit to determine potential stress levels, see Figure 66.

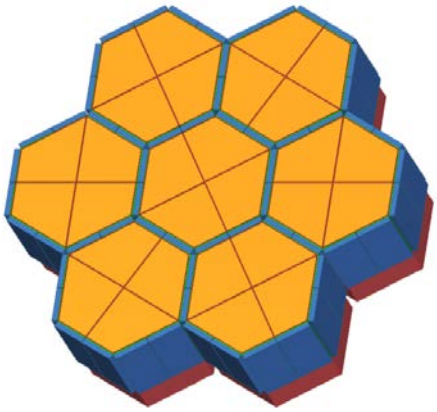

Figure 62: Segmented Polarimeter for High Energy X-rays without lid

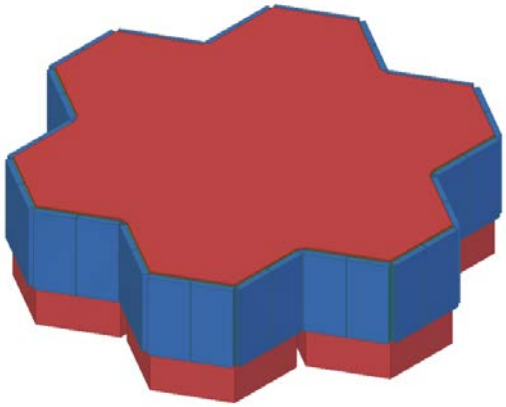

Figure 63: Segmented Polarimeter for High Energy X-rays with lid

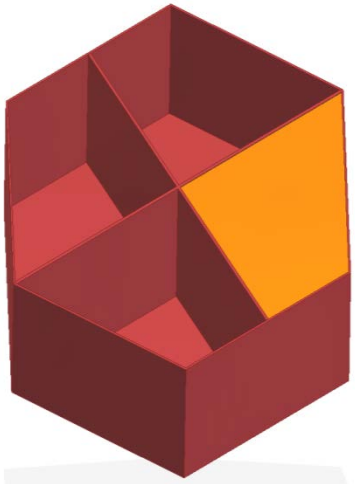

Figure 64: CFRP honey comb structure with one of the four plastic scintillator and PMT(detailed in Figure 65)

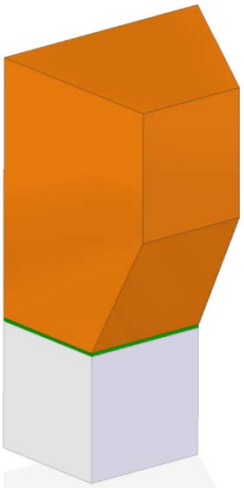

Figure 65: Plastic scintillator attached to PMT with silicone pad.

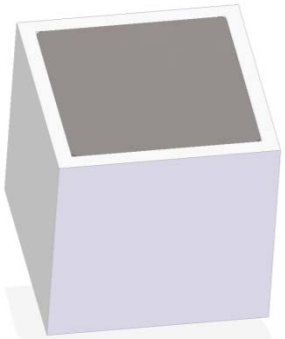

Figure 66: Modelled PMT with borosilicate glass on top

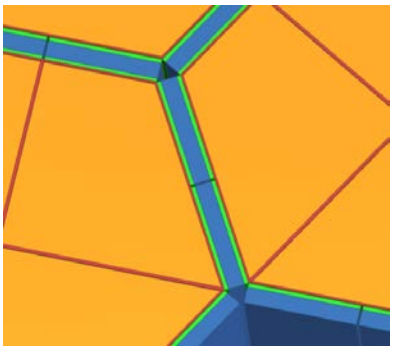

Figure 67: Closer view of placement of silicone pads to mount the BGO on the CFRP

Meshing and contact

The structure has been meshed with different element types listed in Table 26.

Table 26: Meshing parameters

Element name	Number of nodes per element	Degree of freedom per node	Structural components meshed with element type
SOLSH190	4	3	Silicone BGO Silicone PMT Lid Borosilicate Glass BGO
SOLID187	10	3	PMT plastic scintillator
SOLID 186	20	3	CFRP
TARGE170	N/A	N/A	All bounded contacts
CONTA174	N/A	N/A	

Due to restriction in the non-commercial license, a coarse mesh was first implemented. Secondly solid elements have been replaced by solid shell elements, reducing the total number of nodes. Finally refinements could be implemented in sensitive contact areas, between the lid and the CFRP components and between the PMT and the glass. A sensitivity analysis on mesh size of only one unit has been conducted on the modal frequencies, see Appendix 6. The analysis concluded that the modal frequencies are increasing by 10% in average when reducing the number of nodes by 42% and increasing the number of elements by 102% from the initial coarse mesh. The final mesh is shown in Figure 68.

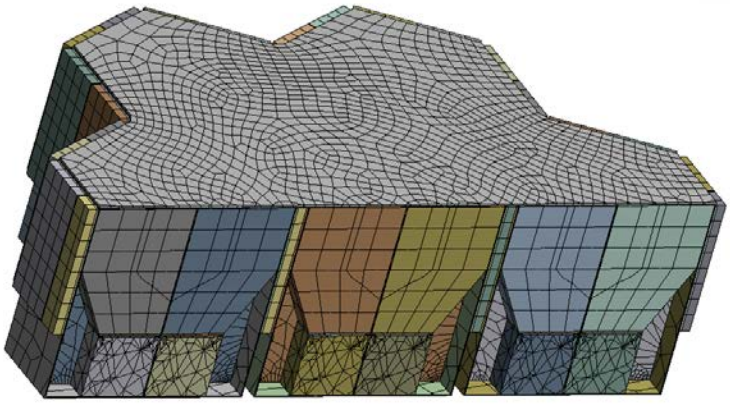

Figure 68: Meshing of the polarimeter with section cut.

As our analysis is linear, the model has been created with only bounded/no slip contact due to which is to say that the slave node should follow the master node.

The lid is attached to the structure as it is fixed only to the honey comb with cross structure. The contact area between the structures is very small as the thickness of the honey comb respective cross is 0.5 and 0.75 mm, see Figure 69.

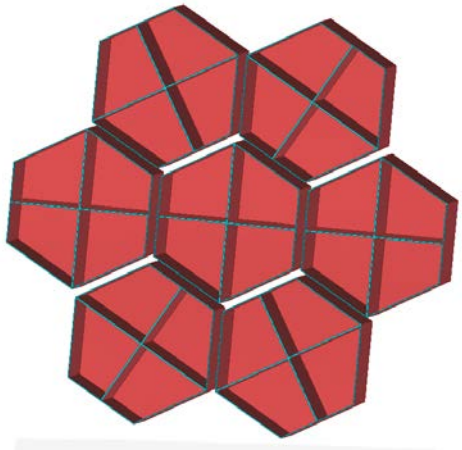

Figure 69: Contact area between lid and honey comb structure shown in cyan.

As a consequence some stress concentration can be observed in the different simulations and would have required a finer mesh. Due to mesh restrictions, these stress concentration points could not be meshed accurately. Furthermore, as no manufacturing assessment of this structure been conducted at this time at this time, it is highly possible that the contact area between the lid and the honey comb structure has been underestimated. Therefore, the stress concentration points in this contact region have been discarded in the results.

Boundary conditions

The structure is modelled with all the units as the structure is not symmetric. Applying symmetry condition in this case would introduce an artificial constrain. The base is fixed; all degrees of freedom are constrained, see dashed area in Figure 70. The base is then excited by an acceleration.

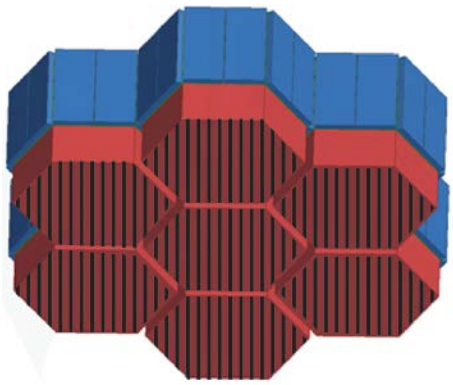

Figure 70: Base of the SPHINX fixed to satellite (dashed lines)

Loading

Random vibration

The structure is excited at its base using NASA's qualification level spectrum ASD [1] in the x-, y- and z- direction at the same time to calculate the RMS von Mises stress as per 2.1.4.2. When comparing stress levels obtained with a random vibration analysis to Mile's equation, the structure is excited in one direction at a time as Mile's equation is based on a SDOF assumption.

Table 27: NASA Acceleration spectrum density for qualification level, instrument under 22.7 kg [1]

Frequency [Hz]	**ASD Level [g^2/Hz]**
20	0.026
50	0.16
800	0.16
2000	0.026

Spectrum for pyro shock

The shock spectrum used is given by [16]. The structure is excited in the x-, y- and z-direction.

Table 28: Shock spectrum

Frequency [Hz]	**Shock spectrum acceleration [g]**
100	15
200	40
500	175
1000	500
5000	500

Results

Modal analysis

The modal frequencies are extracted in accordance to the frequency range of the excitation. For the random vibration analysis, only few modes are within the range of the input excitation. For the shock spectrum analysis, the frequency range is to be 1.5 the frequency range of the input excitation [19]. The resulting frequencies are not presented here. The modal participation factors (PF) are extracted for each stiffness value of the PMT to see which modes will be most excided during the base excitation, see Figure 72 and Table 29.

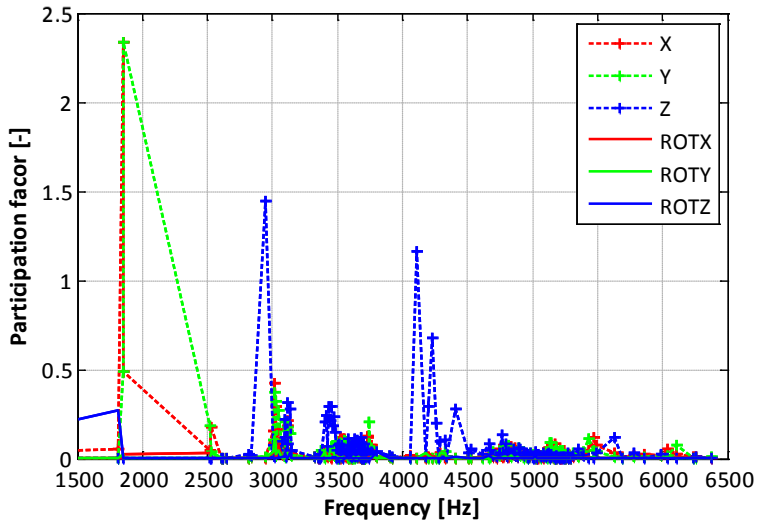

Figure 71: Participation factor as a function of the natural frequencies for a PMT stiffness value of 5 GPa.

The 5 first modes are plotted and compared in Figure 72 and

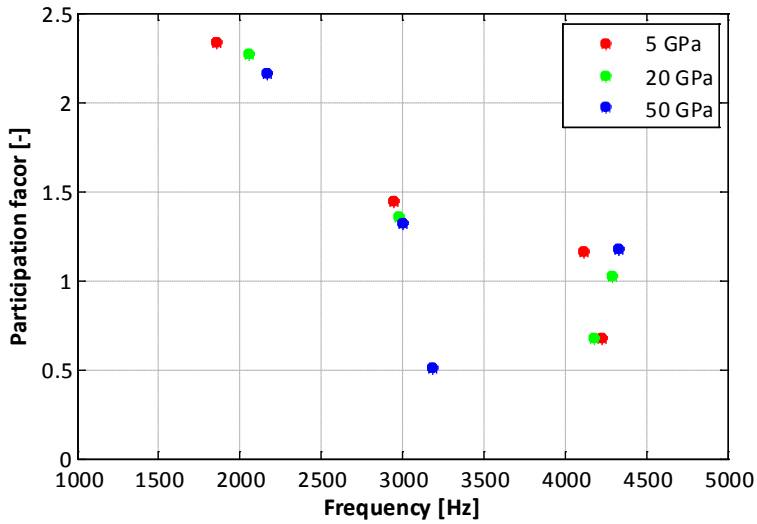

Figure 72: Participation factors for the different PMT stiffness values

Table 29: Participation factors of the 5 most predominant modes for the 3 PMT stiffness values

	PMT Young's modulus [GPa]					
	5		20		50	
	Frequency [Hz]	PF [-]	Frequency [Hz]	PF [-]	Frequency [Hz]	PF [-]
1st predominant mode	1854	2.33	2053	2.27	2165	2.16
2nd predominant mode	1854	2.33	2054	2.27	2166	2.16
3rd predominant mode	2942	1.45	2979	1.36	2996	1.32
4th predominant mode	4109	1.16	4291	1.03	4327	1.18
5th predominant mode	4226	0.68	4178	0.68	3180	0.51

Actual maximum stress value

As some stress concentration points have been observed in the contact region between the lid and the honey comb structure, this value has been discarded as explained in the previous paragraphs. With the concentration points excluded, the highest stress value found is situated at the bottom of the honey comb carbon fiber structure, see Figure 73.

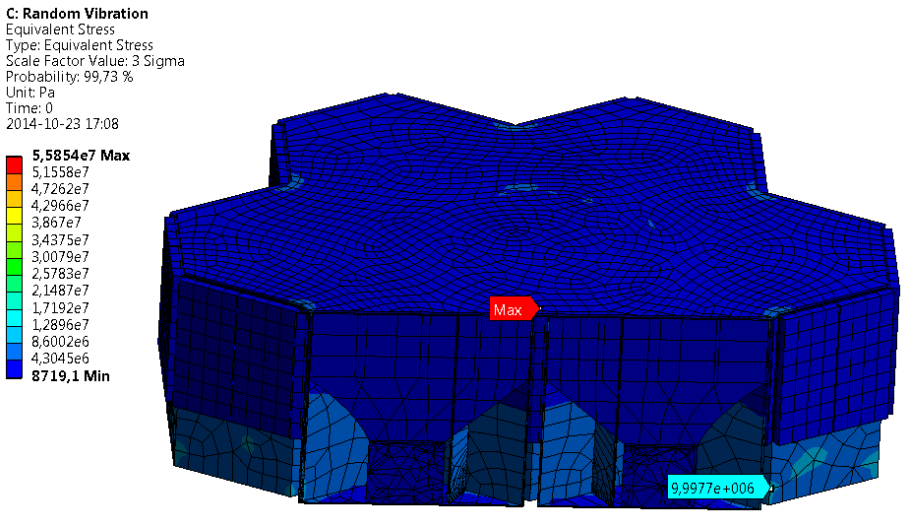

Figure 73: 3σ RMS von Mises values after random vibration load – PMT 5GPa. Stress concentration point due to contact with lid shown as max value. Actual maximum value is shown in blue.

Random vibration

Excitation in 3 directions and parameter study: stiffness PMT

The PMT stiffness being estimated, a sensitivity analysis has been performed to determine the impact on the resulting RMS von Mises stress after random vibration load. The 3σ RMS von Mises stress is then reviewed for all components, for the 3 values of the Young's modulus of the PMT component, to determine if the level of stress generated by the random vibration spectrum would generate plasticity, see Table 30. The stress distribution for a PMT stiffness of 5 GPa can be found for each component in Appendix 4.

Table 30: Maximum RMS von Mises stress for random vibration excitation in 3 directions depending on the Young's modulus of the PMT

Max RMS Von Mises stress [MPa]	**PMT Young's modulus [GPa]**			**Material yield strength [MPa]**
Component	**5**	**20**	**50**	
Glass	2.14	1.84	1.42	35
Lid	9.34	6.51	5.12	350
Plastic scintillator	0.46	0.33	0.27	80
CFRP	10.01	5.93	5.90	350
Silicone BGO	0.09	0.08	0.07	5
BGO	0.37	0.24	0.19	N/A
PMT	1.05	1.85	2.98	40
Silicone PMT	0.08	0.06	0.05	5

Mile's

As Mile's equation was developed for a SDOF only one direction excitation are considered here. The maximum values for the RMS von Mises stress extracted from the Ansys simulations, and excluding contact concentration points, are compared to the von Mises stress obtained after the static GRMS acceleration is applied on the structure, see Figure 74 and Figure 75.

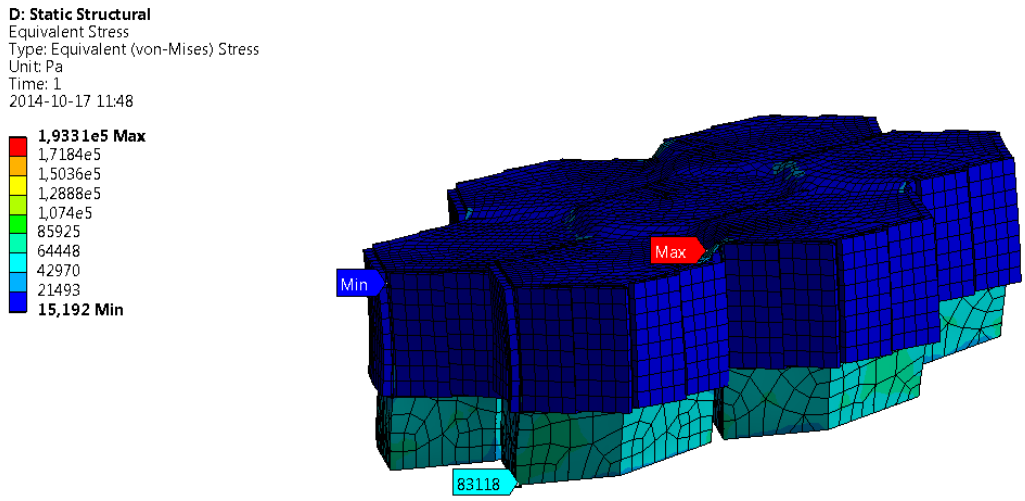

Figure 74: Von Mises stress for 1G acceleration load in x-direction

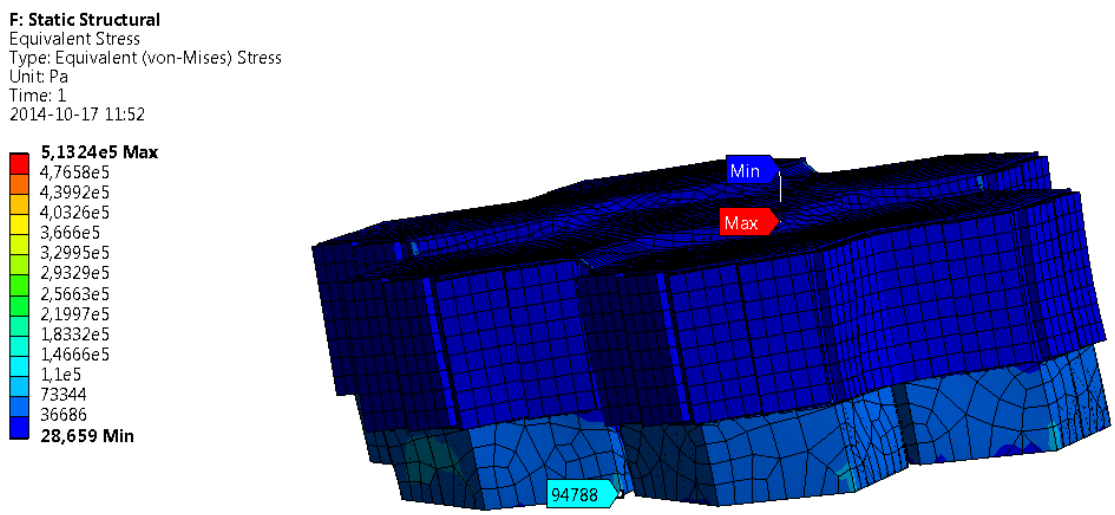

Figure 75: Von Mises stress for 1G acceleration load in y-direction

The results are given for an excitation in x-direction respective in y-direction in Figure 76 and Figure 77.

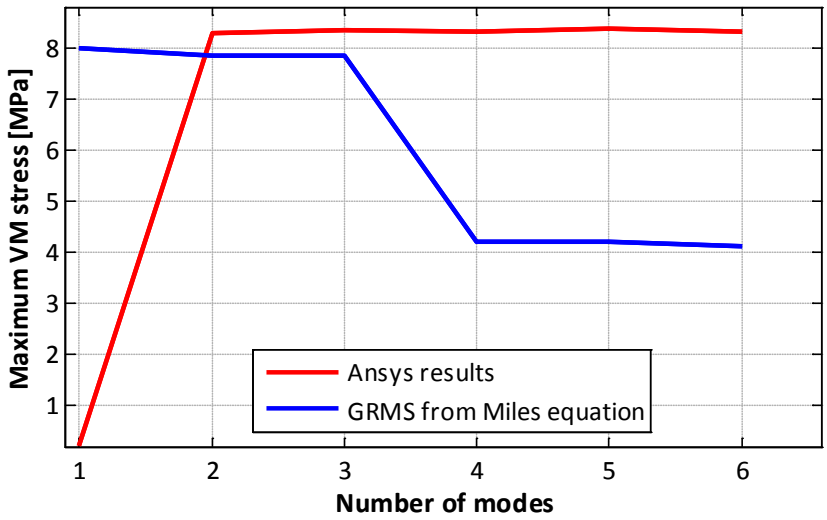

Figure 76: Comparison between Maximum Equivalent von Mises Stress obtained by simulation in Ansys and the stress obtained after applying an equivalent GRMS from Mile's equation on the structure – **X direction**

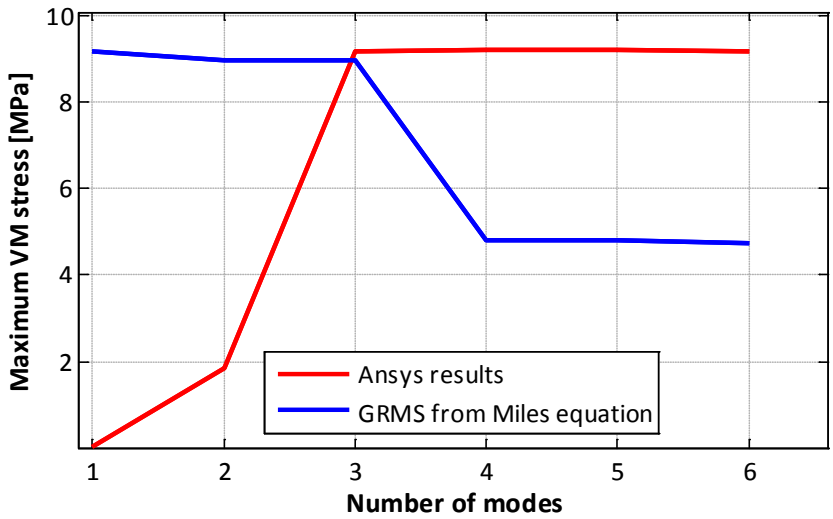

Figure 77: Comparison between Maximum Equivalent von Mises Stress obtained by simulation in Ansys and the stress obtained after applying an equivalent GRMS from Mile's equation on the structure – **Y direction**

Shock spectrum response analysis

As for the random vibration load, the 3σ RMS von Mises stress is reviewed for all components for the shock spectrum see Table 31. The stress distributions are shown in Appendix 4.

Table 31: Safety factors for all components for shock spectrum excitation in 3 directions depending on the stiffness of the PMT

Component	PMT Young's modulus [GPa] 5			PMT Young's modulus [GPa] 20			PMT Young's modulus [GPa] 50		
	Max Von Mises stress [MPa]	Yield strength [MPa]	Safety factor	Max Von Mises stress [MPa]	Yield strength [MPa]	Safety factor	Max Von Mises stress [MPa]	Yield strength [MPa]	Safety factor
Glass	48.6	35	**0.7**	68.0	35	**0.5**	65.1	35	**0.5**
Lid	234.3	350	**1.5**	256.0	350	**1.4**	268.2	350	**1.3**
Plastic scintillator	20.9	80	**3.8**	20.3	80	**3.9**	20.7	80	**3.9**
CFRP	420.6	350	**0.8**	441.1	350	**0.8**	314.2	350	**1.1**
Silicone BGO	8.6	5	**0.6**	8.4	5	**0.6**	8.6	5	**0.6**
BGO	40.6	N/A	**N/A**	45.3	N/A	**N/A**	41.5	N/A	**N/A**
PMT	27.7	40	**1.4**	80.9	40	**0.5**	154.3	40	**0.3**
Silicone PMT	2.3	5	**2.2**	2.7	5	**1.8**	2.7	5	**1.8**

The stress concentration factor in the borosilicate glass and the BGO is also investigated, see Table 32.

Table 32: Safety factors for the borosilicate glass and the BGO for shock spectrum excitation in 3 directions depending on the stiffness of the PMT

Component	PMT Young's modulus [GPa]	Max RMS Von Mises stress [MPa]	Calculated Max stress concentration KI [MPa $m^{1/2}$]	Fracture toughness [MPa $m^{1/2}$]	Safety factor
Borosilicate glass	5	4.86E+01	4.66E-01	0.85	**1.8**
	20	6.80E+01	6.53E-01	0.85	**1.3**
	50	6.51E+01	6.25E-01	0.85	**1.4**
BGO	5	4.06E+01	3.90E-01	0.67	**1.7**
	20	4.53E+01	4.35E-01	0.67	**1.5**
	50	4.15E+01	3.99E-01	0.67	**1.7**

Discussion

Table 30 shows that the structure would not sustain any initiation of plastic deformation under random vibration loading for a 3σ analysis. The shock response spectrum results show a possible weakness of the structure in the carbon fiber honey comb structure and should be considered for further design stages. However, due to the silicone components in this model, the actual damping factor should be tested and checked against the assumed damping factor of 5 % used in these simulations.

Some contact aspects between the lid and the carbon fiber walls have been of concern because of stress concentration areas that do not appear to be physically plausible.

The stiffness of the PMT should be tested. The assumed value, and in particular the lowest value of 5 GPa seems unrealistically low when considering the real structure.

This structure is in a very primarily design stage and some design assumptions have been taken regarding for example silicone addition between the parts. These assumptions should be compared to manufacturing capabilities.

Appendix 4 SPHiNX results

Random vibration analysis with PMT stiffness of 5 GPa – 3σ RMS von Mises stress levels

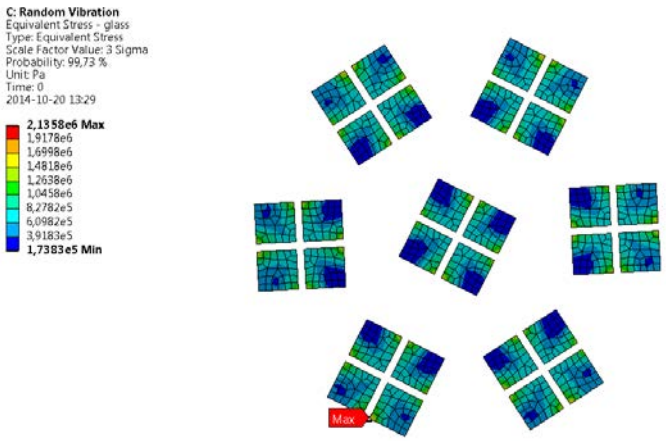

Figure 78: 3σ RMS von Mises stress for the glass components

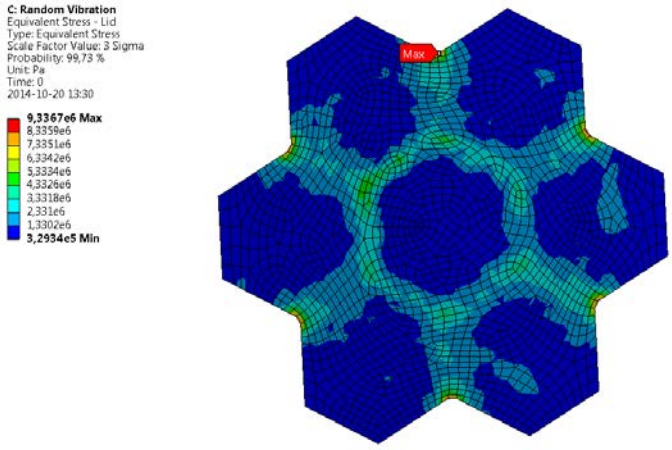

Figure 79: 3σ RMS von Mises stress for the lid

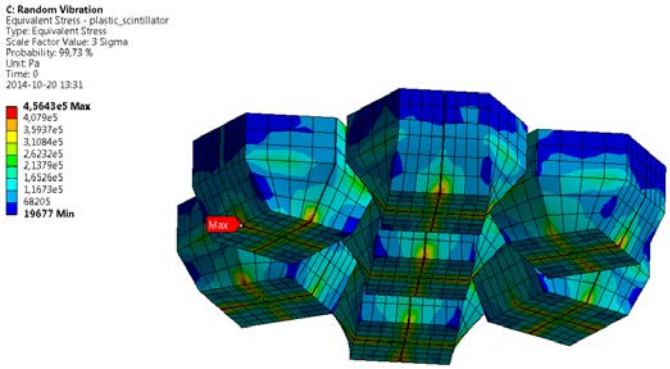

Figure 80: 3σ RMS von Mises stress for plastic scintillators

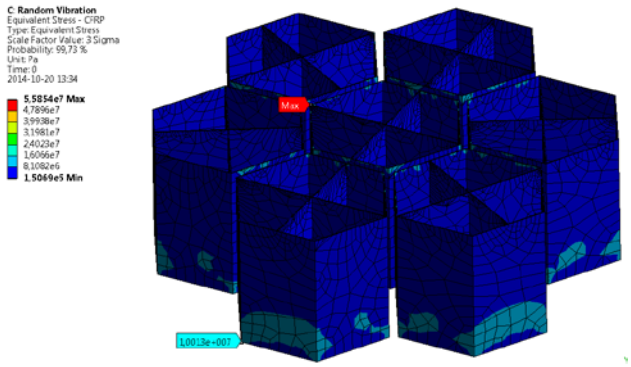

Figure 81: 3σ RMS von Mises stress for honey comb structure

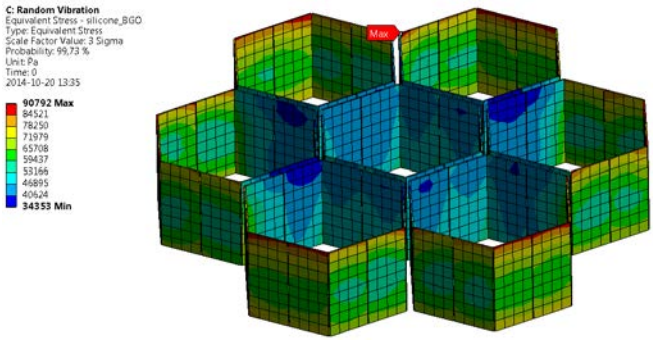

Figure 82: 3σ RMS von Mises stress for the BGO

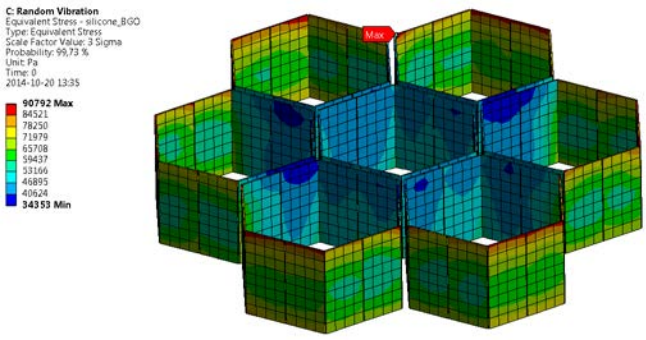

Figure 83: 3σ RMS von Mises stress for the silicone BGO

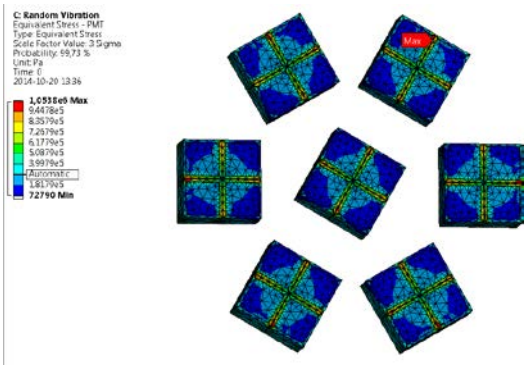

Figure 84: 3σ RMS von Mises stress for the PMT

SPHiNX – Shock spectrum analysis with PMT stiffness of 5 GPa – 3σ RMS von Mises stress levels

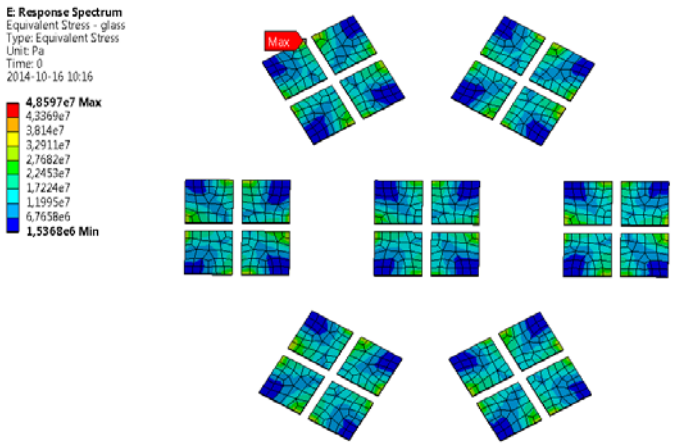

Figure 85: 3σ RMS von Mises stress for the glass components

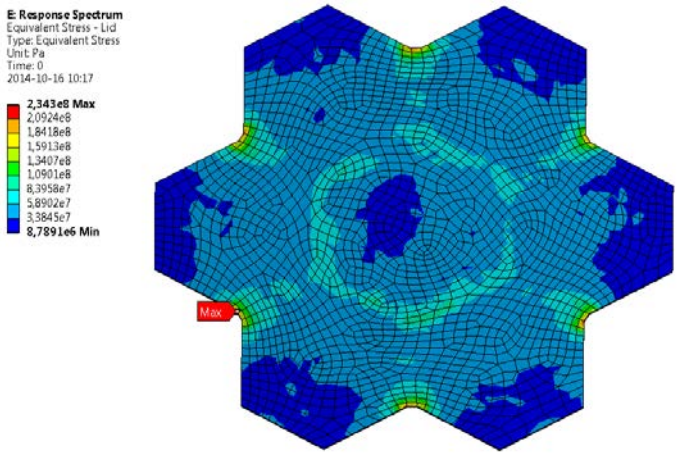

Figure 86: 3σ RMS von Mises stress for the lid

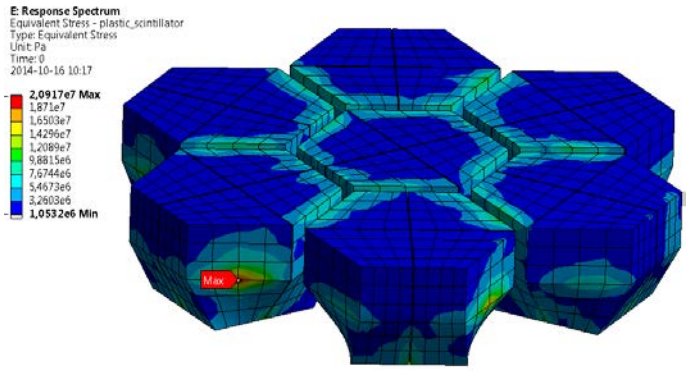

Figure 87: 3σ RMS von Mises stress for plastic scintillators

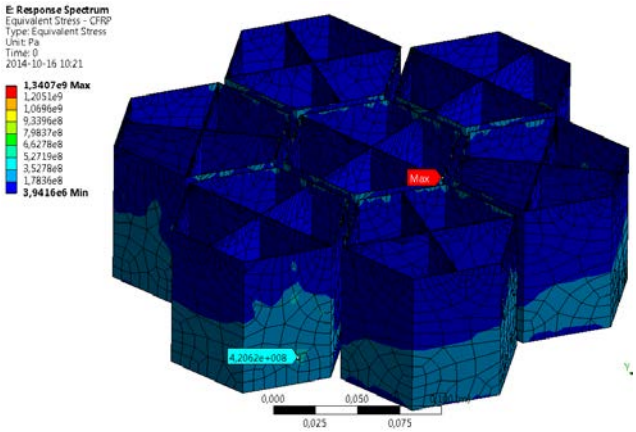

Figure 88: 3σ RMS von Mises stress for honey comb structure

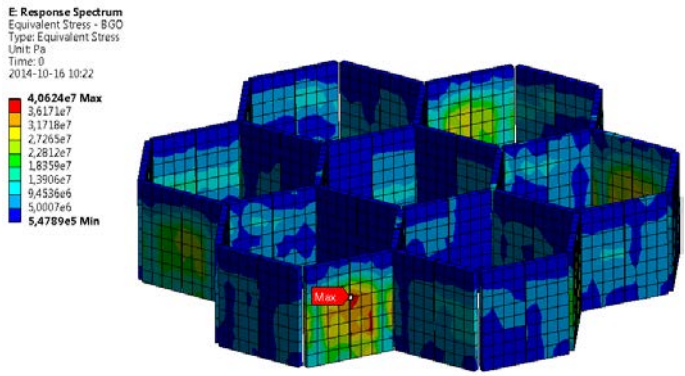

Figure 89: 3σ RMS von Mises stress for the BGO

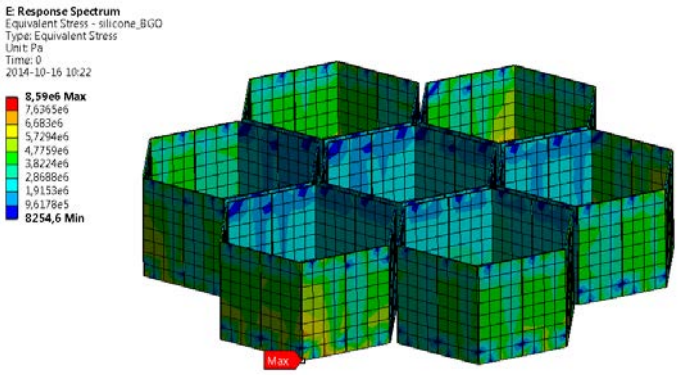

Figure 90: 3σ RMS von Mises stress for the silicone BGO

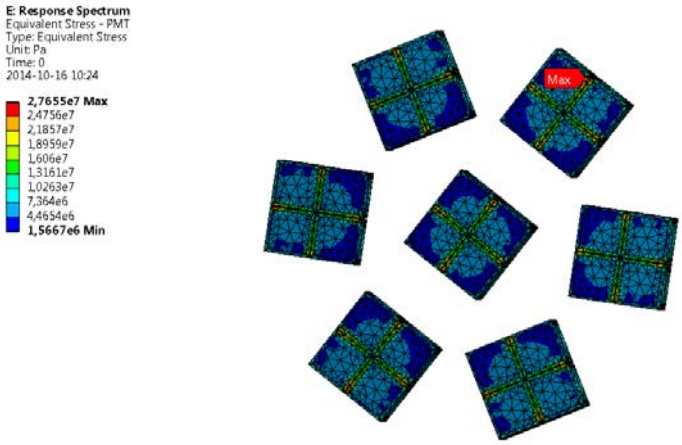

Figure 91: 3σ RMS von Mises stress for the PMT

Appendix 5 Safety factor against fracture

Since the directional results from random vibration analysis are statistical in nature they cannot be combined in the usual way. For example the X, Y, and Z displacements cannot be combined to get the magnitude of the total displacement. The same holds true for other derived quantities such as principal stresses.

As some brittle components made out of glass for example are of interested in the following simulations, a conservative method has been developed to determine a safety factor against fracture using von Mises stress.

The principal criteria in fracture mechanics is the principal stress [24]. A crack will increase when subjected to tension perpendicular to the crack for the first opening mode, when forces are of interest for the second and third modes, see Figure 92.

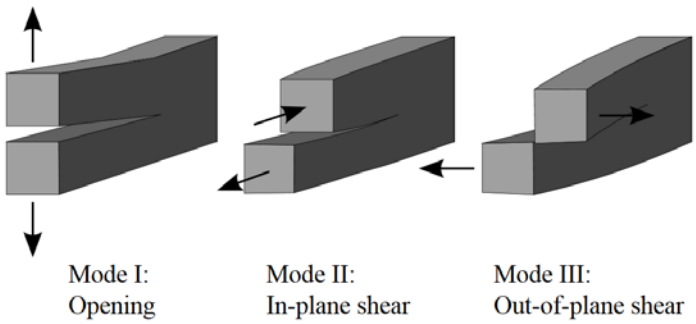

Figure 92: Crack opening modes

In order to estimate if the plasticity criteria, the von Mises equivalent stress, can also be of use to estimate if a structure is dimensioned against crack growth, the von Mises and principal stress criteria are compared in Table 33 .

Von Mises stress is superior or comparable to the maximum value of the principal stress in tension except for a hydrostatic pressure case.

Table 33: Comparison between von Mises and principal stress criteria

Loading case	Von Mises stress	Principal stresses
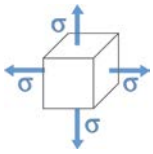	$\sigma_{VM} = \sigma$	$\sigma_1 = \sigma$, $\sigma_2 = \sigma$, $\sigma_3 = 0$ $\max(\sigma_i) = \sigma$
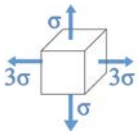	$\sigma_{VM} = \sqrt{7}\sigma = 2.65\sigma$	$\sigma_1 = 3\sigma$, $\sigma_2 = \sigma$, $\sigma_3 = 0$ $\max(\sigma_i) = 3\sigma$
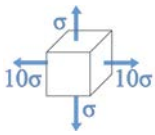	$\sigma_{VM} = \sqrt{91}\sigma = 9.53\sigma$	$\sigma_1 = 10\sigma$, $\sigma_2 = \sigma$, $\sigma_3 = 0$ $\max(\sigma_i) = 10\sigma$
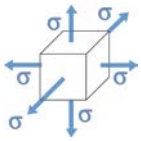	$\sigma_{VM} = 0$	$\sigma_1 = \sigma$, $\sigma_2 = \sigma$, $\sigma_3 = \sigma$ $\max(\sigma_i) = \sigma$
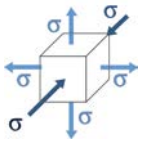	$\sigma_{VM} = 2\sigma$	$\sigma_1 = \sigma$, $\sigma_2 = \sigma$, $\sigma_3 = -\sigma$ $\max(\sigma_i) = \sigma$
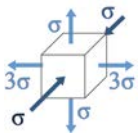	$\sigma_{VM} = 2\sqrt{3}\sigma = 3.46\sigma$	$\sigma_1 = 3\sigma$, $\sigma_2 = \sigma$, $\sigma_3 = -\sigma$ $\max(\sigma_i) = 3\sigma$
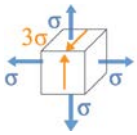	$\sigma_{VM} = 2\sqrt{7}\sigma = 5.29\sigma$	$\sigma_1 = 0.5\left(1+\sqrt{37}\right)\sigma = 3.54\sigma$, $\sigma_2 = \sigma$, $\sigma_3 = 0.5\left(1-\sqrt{37}\right)\sigma = -2.54\sigma$ $\max(\sigma_i) = 3.54\sigma$
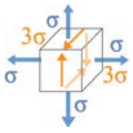	$\sigma_{VM} = \sqrt{55}\sigma = 7.42\sigma$	$\sigma_1 = 0.5\left(1+\sqrt{73}\right)\sigma = 4.83\sigma$, $\sigma_2 = \sigma$, $\sigma_3 = 0.5\left(1-\sqrt{73}\right)\sigma = -3.83\sigma$ $\max(\sigma_i) = 4.83\sigma$
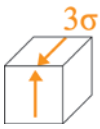	$\sigma_{VM} = 3\sqrt{3}\sigma = 5.20\sigma$	$\sigma_1 = 3\sigma$, $\sigma_2 = 0$, $\sigma_3 = -3\sigma$ $\max(\sigma_i) = 3\sigma$

In order to assess the component's toughness against fracture we assume that the glass with thickness t includes an initial defect of penny shape form [23], with an initial length $2c$ of approximately 20 µm and a height $2a = c$ [22]. The maximum stress concentration factor K_{Imax} is given by [16]

$$K_{\mathrm{I}max} = \sigma_0 \sqrt{\pi a}\, f_8\left(\frac{a}{c}, \frac{a}{t}\right) \tag{65}$$

where σ_0 is the stress perpendicular to the length of the crack. The value of the total von Mises stress σ_{VMtot} is used as σ_0. The factor f_8 is given by

$$f_8\left(\frac{a}{c}, \frac{a}{t}\right) = Q^{-1/2}\left[M_1 + M_2\left(\frac{a}{t}\right)^2 + M_3\left(\frac{a}{t}\right)^4\right] \tag{66}$$

In our case $t \gg a$ and therefore the equation can be simplified to

$$f_8\left(\frac{a}{c}, \frac{a}{t}\right) = Q^{-1/2} M_1 \tag{67}$$

where

$$M_1 = 1 \tag{68}$$

and

$$Q = 1 + 1.464(a/c)^{1.65} \tag{69}$$

The safety factor against damage η_f is calculated with the K_{Ic} is the fracture toughness of the material as

$$\eta_f = \frac{K_{Ic}}{K_{\mathrm{I}max}} \tag{70}$$

where K_{Imax} is the maximum stress concentration factor.

Appendix 6 Mesh quality sensitivity analysis

Table 34: Meshing sensitivity analysis on modal frequencies

Number of nodes	136751	106223	105754	105754	105754	77152	79312	79572	**-42%**
Number of elements	36669	35649	35682	35682	35682	69765	70785	73993	**102%**
Additional meshing step		SWEEP method - Solid shell elements on silicone and BGO	SWEEP method - Solid shell elements on lid	SWEEP method - Solid elements on PMT	SWEEP method - Solid elements on plastic scintillator	SWEEP method - CFRP middle node dropped	Mapped mesh on BGO, silicone, PMT	Refinement on lid mesh	
Modal frequencies [Hz]									
1	1 714	1 716	1 726	1 726	1 726	1 834	1 835	1 866	**9%**
2	1 740	1 742	1 754	1 754	1 754	1 840	1 841	1 870	**7%**
3	1 744	1 746	1 759	1 759	1 759	1 844	1 844	1 934	**11%**
4	2 468	2 479	2 493	2 493	2 493	2 612	2 617	2 711	**10%**
5	2 469	2 480	2 494	2 494	2 494	2 613	2 618	2 712	**10%**
6	2 565	2 579	2 592	2 592	2 592	2 717	2 723	2 804	**9%**
7	2 570	2 584	2 597	2 597	2 597	2 721	2 726	2 809	**9%**
8	2 604	2 618	2 632	2 632	2 632	2 763	2 770	2 890	**11%**
								Average	**10%**